MARMARA UNIVERSITY
INSTITUTE FOR GRADUATE STUDIES
IN PURE AND APPLIED SCIENCES

INVESTIGATION OF THE RELATIONSHIP BETWEEN THE TOPOGRAPHY AND THE FLUID CIRCULATION DEPTH ON THE GEOTHERMAL SYSTEMS OF CENTRAL ANATOLIA REGION

SİNAN BURHAN

MASTER THESIS

Department of Environmental Engineering

THESIS SUPERVISOR

Assoc. Prof. Dr. Kamil ERKAN

ISTANBUL, 2024

MARMARA UNIVERSITY

INSTITUTE FOR GRADUATE STUDIES
IN PURE AND APPLIED SCIENCES

INVESTIGATION OF THE RELATIONSHIP BETWEEN THE TOPOGRAPHY AND THE FLUID CIRCULATION DEPTH ON THE GEOTHERMAL SYSTEMS OF CENTRAL ANATOLIA REGION

SİNAN BURHAN

524319992

MASTER THESIS

Department of Environmental Engineering

Thesis Supervisor

Assoc. Prof. Dr. Kamil ERKAN

ISTANBUL, 2024

ACKNOWLEDGMENTS

Foremost, my deepest gratitude goes to The Almighty, for showering me with the strength to complete this journey successfully and enriching me with wisdom along the way.

This accomplishment would not be possible without the invaluable guidance of Assoc. Prof. Dr. Kamil Erkan, whose creativity, patience, and unwavering belief in me served as a constant source of strength. I'm eternally grateful for the opportunity to work under his supervision.

I extend my sincere thanks to Prof. Dr. Mete Tayanç for entrusting me with this opportunity and supporting its progress.

My profound appreciation goes out to the member of my master's thesis jury member, Assoc. Prof. Dr. Kamil Erkan, who meticulously reviewed my work, enriching it with insightful comments.

My profound appreciation goes out to the member of my master's thesis jury member, Prof. Dr. Bülent Akkoyunlu, who meticulously reviewed my work, enriching it with insightful comments.

My profound appreciation goes out to the member of my master's thesis jury member, Assoc. Prof. Dr. İlker Oruç, who meticulously reviewed my work, enriching it with insightful comments.

This study was supported by ÇAYDAG (Environmental, Atmospheric, Geological, and Marine Sciences Research Grant Committee) of TÜBİTAK (Scientific and Technological Research Council of Türkiye), under the program code (1002-B) and project number (122Y397). I would like to extend my gratefulness, thanks, and appreciation for facilitating the needed resources for making the study possible and to conclude successfully.

I owe debt of gratitude to my parents; whose unwavering moral and financial support paved the way for my success. I dedicate this thesis to them, to my siblings who shared this journey with me and kept me going, and to the love of my life who has been my pillar through all the vicissitudes.

January 2024 **Sinan Burhan**

TABLE OF CONTENTS

ÖZET

İÇ ANADOLU BÖLGESİ'NDEKİ JEOTERMAL SİSTEMLERDE TOPOĞRAFYANIN AKIŞKAN DÖNGÜ DERİNLİĞİ İLE İLİŞKİSİNİN ARAŞTIRILMASI

Sürdürülebilir bir gelecek sunan jeotermal enerji, Türkiye'nin İç Anadolu Bölgesi'nde umut verici bir potansiyele sahiptir. Bu potansiyeli harekete geçirmek için sıcak su kaynaklarının konumlarını ve akışkan yollarını belirleyen faktörleri anlamak kritik öneme sahiptir. Bu çalışma, bu mekanizmaları idealize edilmiş koşullar altında sayısal simülasyonlar kullanarak anlamayı amaçlamaktadır.

Bu çalışmada, jeotermal sistem üzerinde yapılan sayısal modelleme simülasyonu, topoğrafya, ısı akısı ve akışkan dolaşımı arasındaki ilginç etkileşimi ortaya koymaktadır. Topoğrafyanın etkisi (zorlanmış konveksiyon) sistem içindeki baskın ısı akışını şekillendirmektedir. Dikkat çekici bir şekilde, daha derin akışkan dolaşımının da taban ısı akısının büyüklüğünden etkilendiği, akışkan dolaşımının dinamik bir yapıya sahip olduğu gözlemlenmiştir.

Bu çalışmanın bulguları, basitleştirilmiş koşullar altında bile bazal ısı akısının fay zonu sıcaklıkları üzerindeki önemli etkisini göstermektedir. Simülasyonlarda topoğrafı yükseklik için 0 ile 1500 metre arasında kullanılmıştır. Ayrıca, Nusselt sayısı ve saha verileri referans modeli ile bazal ısı akısı, 65 $mW \cdot m^{-2}$ (İç Anadolu Platosu) ve 110 $mW \cdot m^{-2}$ (Kırşehir Masifi) için karşılaştırılmıştır. Topoğrafı yükseklik yaklaşık 1000 metrenin üzerine çıktığında Nusselt sayısı değerinin artışı azalmaktadır. Sonuç olarak, topoğrafya, İç Anadolu bölgesinde sıcak su kaynaklarının oluşumlarında önemli bir faktör olarak ortaya çıkmaktadır.

Araştırmada, 32 jeotermal alanda 141 jeotermal kuyudan sıcaklık-derinlik verisi kullanıldı. Var olan verilere dayanarak ve simüle edilen sıcaklık-derinlik profilleri ile karşılaştırılarak bu araştırmanın sonuçları desteklenmiştir. Elde edilen sonuçlar diğer çalışmalarla da uyumludur ve bu çalışmada kullanılan simülasyon yaklaşımını desteklemektedir. Bu çalışma İç Anadolu Bölgesi'nin jeotermal potansiyelinden yararlanmak için bir katkı sunmaktadır.

Anahtar kelimeler: jeotermal enerji, İç Anadolu Bölgesi, topoğrafya, akışkan döngüsü, sıcaklık-derinlik profili

ABSTRACT

INVESTIGATION OF THE RELATIONSHIP BETWEEN THE TOPOGRAPHY AND THE FLUID CIRCULATION DEPTH ON THE GEOTHERMAL SYSTEMS OF CENTRAL ANATOLIA REGION

Geothermal energy offers a sustainable future, and Central Anatolia Region in Türkiye holds promising potential. To unlock this potential, understanding the factors governing hot spring locations and fluid pathways is crucial. This study aims for understanding these mechanisms using numerical simulations under idealized conditions.

In this study, the simulated numerical modeling on geothermal systems reveals an interesting interplay between topography, heat flow, and fluid circulation. The influence of topography (forced convection) shapes the dominant flow of heat within the system. Remarkably, deeper fluid circulation is also observed to be affected by the magnitude of basal heat flow, showing a dynamic nature of fluid circulation.

Intriguingly, findings of this study highlight the significant impact of basal heat flow on fault zone temperatures, even under simplified conditions. In the simulations, the topographic relief between 0-1500 m were used. Nusselt number and field data-reference model were compared for basal heat flow, 65 $mW \cdot m^{-2}$ (Central Anatolia Plateau) and 110 $mW \cdot m^{-2}$ (Kırşehir Massif). Nusselt number rate of increase starts to decrease at topographic relief of above 1000 m. As a result, the topography emerges as an important factor in the formations of hot springs in the Central Anatolia Region.

The temperature-depth data was used from 141 geothermal wells in 32 geothermal fields for investigation. Building upon existing data and comparing with the simulated temperature-depth profiles supports the results of this investigation. The results are in agreement with other studies confirming the simulation approach used, presenting a contribution to harness Central Anatolia Region's geothermal potential.

Keywords: geothermal energy, Central Anatolia Region, topography, fluid circulation, temperature-depth profiles

SYMBOLS

β : Coefficient of thermal expansion of fluid (K^{-1})

ρ : Mass density of fluid ($kg \cdot m^{-3}$)

λ : Thermal conductivity ($W \cdot m^{-1} \cdot K^{-1}$)

ρ_0 : Reference bulk density ($kg \cdot m^{-3}$)

ΔT : Temperature anomaly (°C)

$c\rho$: Heat capacity ($J \cdot kg^{-1} \cdot K^{-1}$)

d_w : Well depth (m)

d_z : Subsurface depth (m)

fz : Fault zone thickness (m)

g : Gravitational acceleration ($m \cdot s^{-2}$)

H : Topographic relief (m)

K : Permeability (m^2)

P : Fluid pressure (Pa)

P_0 : Atmospheric pressure (Pa)

Q_b : Basal heat flow ($mW \cdot m^{-2}$)

T : Fluid temperature (°C)

T_0 : Annual average surface temperature (°C)

T_b : Conductive background temperature (°C)

T_{bw} : Bottom-well temperature (°C)

T_w : Well temperature along the depth (°C)

T_{wh} : Well-head temperature (°C)

v : Fluid velocity in ($m \cdot s^{-1}$)

μ : Dynamic viscosity of fluid (Pa·s)

σ : Heat capacity ratio

ABBREVIATIONS

CA : Central Anatolia

CAP : Central Anatolia Plateau

EGS : Enhanced Geothermal Systems

FEM : Finite Element Method

GVC : Galatian Volcanic Complex

KM : Kırşehir Massif

MTA : Mineral Research and Exploration General Directorate

MW : Megawatt

Myr : Million year

NAF : North Anatolian Fault

Nu : Nusselt number

T-D : Temperature-Depth

LIST OF FIGURES

LIST OF TABLES

Page

1. INTRODUCTION

In recent years, geothermal resources have gained significant importance due to their low-carbon footprint, renewable, and base-load energy. Geothermal energy is suitable to be utilized and adopted in multiple sectors according to the available fluid temperature in the geothermal system. High-temperature geothermal sources, 150 °C and above are suitable to be utilized for electricity generation, while lower-temperature, between 40 and 150 °C geothermal sources are suitable in direct use such as residential heating, greenhouse cultivation and various industrial applications (Mock et al., 1997).

Within the scope of transition to global climate change, adaptation of non-traditional resources such as hot rock, and deep sedimentary formations have emerged as a significant strategy along with the traditional geothermal resources of hydrothermal and igneous systems (Mock et al., 1997; Tester, 2007). Presently in Türkiye, as of 2020 (ETKB, 2021), energy production of 1613 MW in electricity and 3495 MW in thermal are produced through geothermal resources (Şimşek, 2009).

In addition to the observational studies, numerical modelling studies have received attention in recent years (Guillou-Frottier et al., 2013; López and Smith, 1995; Magri et al., 2016; McKenna and Blackwell, 2004; Pearson-Grant and Bertrand, 2021; Person et al., 2012; Taillefer et al., 2018; Wisian and Blackwell, 2004). These studies contribute to an enhanced comprehension of the occurrence of both surfaces, such as hot water resources, and non-surface deep geothermal resources. To reduce the high risk from drilling activities in geothermal energy investments, transport mechanisms of geothermal fluid are critical to comprehend and elucidate geothermal resources and developments. Insufficient data in subsurface and deep surface in geothermal fields have led to the data limited to topography, structural measurements, and surface measurements (hot springs) temperatures. Insights and data of regional lithological structure, permeability (K), and complex developments of deep processes in geothermal systems, are yet to be manifested. Nonetheless, numerical modelling shed light on opportunities for understanding the fluid circulation structure in deep layers of hydrothermal activity.

Türkiye has emerged among the top countries of reliable geothermal resources due to its proximity to active tectonic plates of the world. In terms of geothermal resources and production, Aegean Region, in western Türkiye, or western Anatolia such as Gediz

and Büyük Menderes grabens are leading, followed by Central Anatolia (CA) Region and Eastern Anatolia Region (Hepbasli and Ozgener, 2004; Serpen et al., 2009). In Türkiye, Aegean Region dominates well-established geothermal resources, possessing promising potential on world stage (Hepbasli and Ozgener, 2004). Extensive literature is conducted in western Türkiye resulting in establishment of geothermal power plants and direct district heating (Erdogmus et al., 2006; Serpen et al., 2009). The highest fluid temperatures in geothermal systems are found in western Türkiye. Faulds et al., (2009); Söğüt et al., (2010) suggests that in Türkiye, deep circulation of hydrothermal fluids of meteoric origin is the primary control on the geothermal systems such as is the case in Salihli, Manisa.

In conjunction with western Türkiye studies (Faulds et al., 2010; Mutlu, 1998; Söğüt et al., 2010; Tarcan et al., 2005; Uzelli et al., 2021) in topography and hydrogeochemical aspects of the geothermal systems, a comprehensive approach is to focus on remaining regions of Türkiye to complement western Türkiye and promote sustainable energy throughout Türkiye, beginning with the promising potential of CA Region. Although many hydrogeochemical studies (Akıllı and Mutlu, 2018; Pasvanoğlu and Çelik, 2018; Şener et al., 2023; Şener and Baba, 2019; Ünsal and Afşin, 1999) are available for the CA Region; topography and fluid circulation depth studies on geothermal systems in CA Region have been very limited.

To address energy requirements of Türkiye, geothermal resources in the CA Region play significant role in development of geothermal energy infrastructure, concurrent with facilitating transition to low-carbon emissions and addressing sustainable energy action plan of the European Green Deal (Hoogland et al., 2019; Igliński et al., 2022; Karlsdottir et al., 2020; Miłek et al., 2022). Perhaps, in addition, Limberger et al. (2018) provides an insight of how topography of world can improve and develop geothermal energy production globally.

1.1. Central Anatolia Region

In the heart of Türkiye, CA Region covers 151,000 km^2, comprising 21% of the territory in Türkiye (Altın et al., 2012), exhibiting a contrast of topography between its lowlands and highlands, ranging in the heights of as low as 680 m above sea level, with some exceptional peaks of Erciyes (3916 m), Aladağlar mountain range, Hasan Dağı (3253

m) and Karadağ (2271 m) in **Figure 1.1**. Renowned for its tectonic lowlands (known as Ova in Turkish), surrounded by highlands in the vicinity of the region. The lowlands are found in the Konya province, followed by provinces of Ankara, Kayseri, Aksaray, Karaman, Eskişehir and Sivas. The 13 provinces of CA Region are, namely Ankara, Yozgat, Eskişehir, Karaman, Kırıkkale, Çankırı, Niğde, Aksaray, Sivas, Konya, Kayseri, Kırşehir and Nevşehir, are bordered by black solid lines in **Figure 1.1**.

1.1.1. Geologic setting of Central Anatolia Region

The CA Region sits on a complex geological setting, due to the convergence of several tectonic plates. One of the most prominent fault lines in the region is the North Anatolian Fault (NAF), extending right-lateral strike-slip fault type by east-west across northern provinces of the CA Region, signifying the boundary between the Eurasian plate and Anatolian plate (Şengör, 1980), moving at approximately 20 $mm \cdot yr^{-1}$ (Reilinger et al., 2006, 1997) westwards relative to the Eurasian plate (Aydar et al., 1994). In addition, Şengör, (1980); Şengör and Yılmaz, (1981) argue that convergence of African-Arabian and Eurasian plates towards the north provides volcanic activity in the plates involved in the region. The major fault zones existing in CA Region is illustrated by black dashed lines in **Figure 1.1**. The complex neo-tectonic setting of Anatolia is a direct consequence of the ongoing collision between the Eurasian and African plates (Dewey et al., 1973; McKenzie, 1972; Şengör, 1980). Geomorphology of Anatolia and of the vicinity area began to develop in the Late Oligocene-Early Miocene period and continued progressing later throughout the Neotectonics period (Şengör and Yılmaz, 1981).

The boundary of Kırşehir Massif (KM) is illustrated in purple solid lines and the KM granite boundary in maroon solids lines, and any area beyond KM block is the Central Anatolia Plateau (CAP). In addition, northwestern area of the KM block encompasses Kızılcahamam area, known as Galatian Volcanic Complex (GVC) (Görür et al., 1984; Kazancı, 2012; Pasvanoğlu and Çelik, 2018) in **Figure 1.1**. In this study, CA Region will be studied into two different areas, clustered as KM and CAP.

1.1.2. Topography of Central Anatolia Region

In terms of tectonics, the CA Region is a plateau bounded by NAF zone in the east, the Taurus Mountains, which are thrust zone of the Cyprus Arc in the south, and the western Anatolian expansion zone in the west is CAP (Barka and Reilinger, 1997). The eastern boundary of the CAP is continuous towards the Eastern Anatolian Plateau. According to (Cosentino et al., 2012), the present-day topography of CA Region was formed 10 Myr ago, affiliated to 1000 m (Aydar et al., 2013; Yildirim et al., 2011) and above of surface uplift. For initial stages of the study, to visualize the influence of topography on the geothermal resources in the CA Region, distribution map is in **Figure 1.1**.

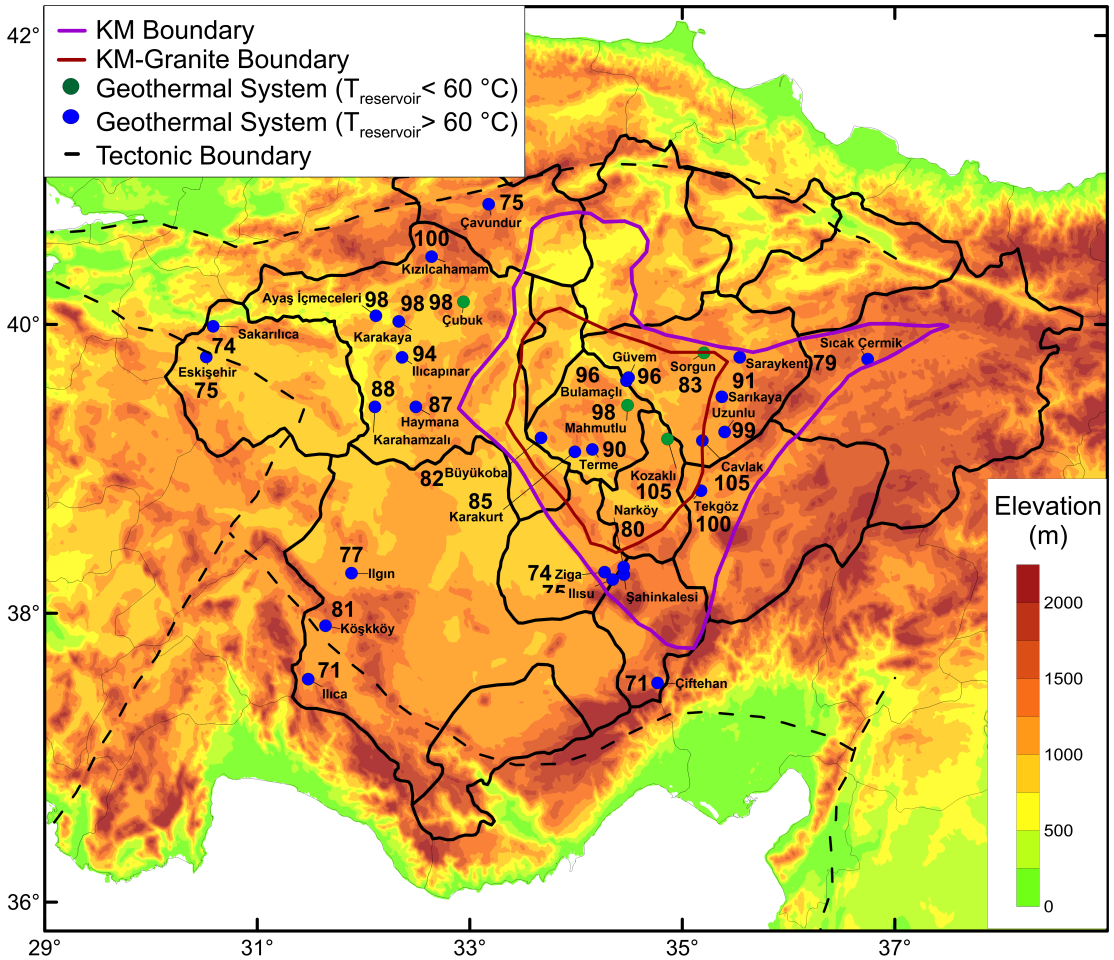

Figure 1.1 Distribution map of geothermal systems in CA Region (Akkuş et al., 2005).

1.1.3. Geothermal resources in Central Anatolia Region

In Türkiye, the known geothermal resources are mainly fault-controlled geothermal systems. Studies suggest that the topography and basal heat flow impose a significant

influence on the geothermal fluid circulation within such systems (Pearson-Grant and Bertrand, 2021; Taillefer et al., 2018; Wisian and Blackwell, 2004). CA Region hosts hot springs, bathing pools and direct usage, also district heating and greenhouse have been established in the region (Parlaktuna et al., 2013).

1.2. Geothermal Systems

In natural convection systems, convection is induced by buoyancy forces that occur due to the increase in the temperature throughout the depth. On the other hand, the effect of topography on the formation of the geothermal systems in fault zones with the pressure-driven flow (forced convection) is demonstrated by different modelling studies Bodri and Rybach, (1998); Forster and Smith, (1989). The modelling studies show that both the natural and forced convection mechanisms contribute to the geothermal system temperatures giving "mixed convection" (Magri et al., 2016; Pearson-Grant and Bertrand, 2021). Although the general proposition of the topography effect is effective at shallow depths for buoyancy forces in natural convection, recent studies have revealed that the topography is effective in the formation of high-temperature geothermal systems derived from deeper depths (Pearson-Grant and Bertrand, 2021; Taillefer et al., 2018).

1.2.1. Permeability in geothermal systems

In most of the fault-controlled geothermal systems, the permeability of the medium is maintained by the fractures, contributing to secondary permeability. On the other hand, bedrock as primary permeability is not a significant factor in terms of the determination of circulation depth (Magri et al., 2016). Numerous geothermal systems are formed in areas lacking aquifers supporting the insignificance of primary permeability. Based on the data obtained from existing geothermal systems, the minimum permeability value of 10^{-16} m^2 is essential for convective heat transfer to initiate in the earth's crust (Manning and Ingebritsen, 1999). As permeability exceeds the previously mentioned value, natural convection occurs. Conversely, even in the areas of lower matrix permeability in the tectonically active geothermal fields, where such low values are easily ensured through presence of fractures. Consequently, it is, therefore, possible to model the circulations of existing geothermal systems by defining an accurate fault and fracture geometry. For instance, Wisian and Blackwell (2004), produced a model of the fluid convection for different regional permeability values by identifying a fault zone that delimits the horst

in the horst-graben structures observed in active tectonic zones. In their study, it was concluded that the convection occurs within a narrow range of 10^{-15} and 10^{-16} m^2 permeability values only. While no convection occurs at lower permeability, at higher permeability, geothermal systems rapidly cool down under surface effects. In addition, the model results demonstrated that the fault zone fluid is not only supplied by the horst bordering the fault zone but also by neighbouring horst, due to topographic relief.

1.2.2. Fluid circulation in geothermal systems

The subsurface groundwater flow pathways and their association with waterbodies are difficult to understand due to invisibility of these pathways from direct observations, as well as hypothetical approach of bedrock as an impermeable layer (Feth, 1964; Frisbee et al., 2013). Conversely, Anderson et al., (1997); Gascoyne and Sheppard, (1993) suggest that to some extent, bedrock is permeable aided by fractures.

In addition, however, Gascoyne and Sheppard (1993) argues that, to some extent, the bedrock is permeable in waterbodies the through fractures. Also, Anderson et al. (1997) suggest that permeability in highland is relatable, even though the waterbody is minimal.

Despite recent advancements in geophysical methods, lack of field data for estimates of fluid circulation depths hindered the progress of the hydrogeologic studies and caused inadequate attained results (Rempe and Dietrich, 2014; St Clair et al., 2015). Such data are pivotal in the development of models involving deep processes and characterize the hydrogeological properties effectively in deep layers (Ball et al., 2014).

For instance, Mayo et al. (2003) reports stratigraphically controlled shallow circulation of 75–300 m and subsurface groundwater of above 700 m. In their study, it has been described the shallow circulation is occurring within active zones of the bedrock, and the deep circulation is occurring within the inactive zones. Due to such constraints, it is challenging to model fluid flow in the bedrock aquifer as some of the bedrock units may allow fluid circulation (Frisbee et al., 2017). Also, their study suggests that topography is non-pivotal for fluid circulation. However, if topographic relief emerges, it supports the fluid circulation, evolving the dynamics of geothermal systems.

1.2.3. Effects of topography in geothermal systems

Groundwater flow is a critical factor in the geothermal systems, applying an influence on the fluid movement, heat transfer and behaviour of geothermal systems. Investigating the groundwater flow dynamics in the geothermal reservoir is essential for sustainable geothermal resources to optimize and manage its utilization. One of the components of efficient groundwater flow in the geothermal system is the topography in facilitating the patterns and pathways of groundwater flow.

In the topographic-driven geothermal systems, the meteoric water infiltrates at high topographic relief, where meteoric waters are warmed at shallow-level crust and quickly rise upwards through permeable fluid pathways of subsurface (Craw et al., 2013; Wisian and Blackwell, 2004).

To a significant extent, the water table is spatially characterized by slightly lower relief coinciding to surface topography, establishing deeper water table depths found beneath high topographic reliefs compared to shallower water table depths found beneath low topographic reliefs (Fetter, 2011). However, despite using the piezometric method and producing maps, direct measurement of the exact water table elevation is challenging. Thus, this approach simplifies boundary conditions of the models. Consequently, water table elevations are estimated through well drilling, producing waterlogs for well data. Groundwater flow caused by topography may be identified by the correlation between elevation and circulation depths (Tóth, 1999).

2. METHODOLOGY

In this study, the Finite Element Method (FEM) was employed to investigate the effect of topography and basal heat flow (Q_b) value on geothermal fluid temperatures. Within the scope of this study, two-dimensional numerical model was developed, introducing the equations, parameters, boundary conditions and geometry in the script code of the program. The outcome results of the model were compared with Wisian and Blackwell (2004) to validate the produced model. Subsequently, well borehole dataset for the CA Region was gathered, including well logs, retrieving data from MTA (Maden Tetkik ve Arama Genel Müdürlüğü, Mineral Research and Exploration General Directorate) and literature. Consequently, referring to MTA inventory book Akkuş et al. (2005), the fault lines existing in the vicinity of the geothermal field were considered for delineation and

topographic relief (H) was calculated for each geothermal field in CA Region in **Figure 1.1**. Within the scope of modelling studies, the Q_b and H parameters were changed for simulation and their effect on the fault zone temperatures was calculated. Temperature-Depth (T-D) profiles were produced along the fault zone and e-profiles meeting the fault zone at some point in the subsurface depth. The obtained results of the numerical model have been evaluated by comparing the conditions in the geothermal systems associated with reservoir temperatures below and above 60 °C in CA Region. Simulation scenarios were analysed and compared with the geothermal field data that had been retrieved in the region.

2.1. Heat Flow Distributions

In CA Region, heat flow measurements have been conducted by a few studies (Balkan-Pazvantoğlu and Erkan, 2019; Tezcan and Turgay, 1991). Balkan-Pazvantoğlu and Erkan (2019) suggests heat flow value of ~65 $mW \cdot m^{-2}$ on average, however, areas such as Kızılcahamam and Kırşehir anomalies have demonstrated a considerably high heat flow, showing a considerable measurement of more than 100 $mW \cdot m^{-2}$. Therefore, in the modelling, two different heat flow values of 65 $mW \cdot m^{-2}$ in CAP and 110 $mW \cdot m^{-2}$ in KM were employed. The relatively high temperatures of geothermal systems in the KM have been attributed to high radioactive heat production of the granites that form the massif (İlbeyli et al., 2004).

2.2. Model Design

A two-dimensional schematic illustration of geological model was considered to demonstrate fault zone, hot spring or geothermal source, basin-fill, and bedrock zones. In addition, the boundary conditions and geometry used in the modelling are in **Figure 2.1**, where the model boundary conditions are designated in black text, thermal transport modelling in red text, and hot spring location in blue text. In the **Figure 2.1**, λ is thermal conductivity, K is permeability, **U** is Darcy velocity, **g** is gravitational acceleration, T is temperature, T_0 is annual average surface temperature, and H is topographic relief.

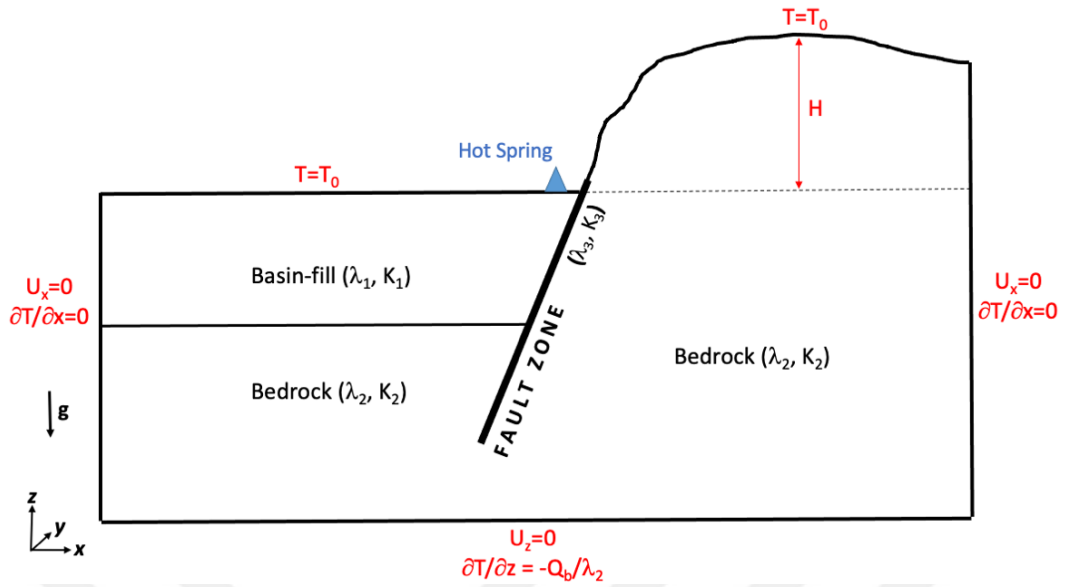

Figure 2.1 Schematic illustration of two-dimensional geological model.

In the simulations produced, thermal irregularities were observed in the model when the heat flow was directly applied at the bottom. To resolve the issue, an impermeable layer of 10^{-20} m^2 was introduced at the bottom of model, a constant temperature was applied to the bottom of the model to provide an analogous heat flow. In addition, Forster and Smith (1989) implemented a similar approach in their study to remediate the thermal irregularities.

2.3. Numerical Modelling

The numerical modelling studies have been carried out utilising a commercial program, FlexPDE (PDE Solutions Inc, 2023), to solve partial differential equations using FEM and the produced outcome results of the model were analysed. The physical equations, or conservation equations, representing dynamics of the environment, model geometry, and boundary conditions necessary for the solution of the equations were defined using program-specific commands to write script code, and then the model was run to produce outcomes. A two-dimensional spatial has been considered as such dimension enables geological and hydrological scenarios to be defined in limited parameters and produce comprehensive results. In addition, the two-dimensional numerical model was adopted to investigate the effect of topographic relief (H) on geothermal systems, effect of the groundwater flow for the various heat flow (Q_b), and permeability (K) scenarios. The meshing automation produced by FlexPDE, and further detail is in **Figure A.2**.

2.3.1. Equations used in model

Fluid movement under certain boundary conditions in permeable medium underground can generally be solved by the Navier-Stokes equations. The problem can be reduced to the Darcy flow problem by using the average velocity of the fluid in the porous medium (Darcy velocity). In modelling, the mechanical and thermal state of the fluid is defined by equations of momentum, mass, and heat conservation, given respectively in (Nield and Bejan, 2006):

$$\nabla P = -\frac{\mu}{K}\mathbf{v} + \rho_f \mathbf{g} \qquad \textbf{Eq. (2.1)}$$

$$\nabla \cdot \mathbf{v} = 0 \qquad \textbf{Eq. (2.2)}$$

$$(c\rho)_m \frac{\partial T}{\partial t} + (c\rho)_f \mathbf{v} \cdot \nabla T = \lambda \nabla^2 T \qquad \textbf{Eq. (2.3)}$$

In these equations, P represents fluid pressure, μ represents dynamic viscosity of the fluid, K represents permeability, ρ represents mass density of fluid, **v** represents fluid velocity (Darcy velocity), $c\rho$ represents heat capacity of matrix (m) and fluid (f), T represents fluid temperature, λ represents coefficient of thermal conductivity of medium, and **g** represents gravitational acceleration. In addition to above equations, in **Eq. (2.1)**, the temperature-dependent change of the density of fluid is (Nield and Bejan, 2006):

$$\rho_f = \rho_0(1 - \beta(T - T_0)) \qquad \textbf{Eq. (2.4a)}$$

In the equation, T_0 represents annual average surface temperature, ρ_0 represents reference bulk density and β represents coefficient of thermal expansion of fluid, for the viscosity of the fluid given in **Eq. (2.1)** (Rabinowicz et al., 1998):

$$\mu = 2.414 \times 10^{-5} \times 10^{\frac{247.8}{(T+199)}} \qquad \textbf{Eq. (2.4b)}$$

formula has been used. The remaining physical parameters such as the coefficient of thermal expansion of fluid (β), and heat capacities of fluid ($c\rho$) were retrieved from Stauffer et al. (1997).

In the simulations, conductive heat equation for ambient initial temperature distribution was solved to respect-sent the initial thermal conditions. In addition, the hydrostatic

pressure condition is accepted for the initial pressure distribution. Under the initial and boundary conditions described above, equations for ambient temperature and pressure (**Eq. 2.2** and **Eq. 2.3**) are solved sequentially. The distribution of Darcy velocity after each successive solution was calculated using **Eq.** (**2.1**).

2.3.2. Boundary conditions of model

In the model, the upper boundary is at a constant atmospheric pressure (P_0) of 10^5 Pa and T_0 of 20 °C. Whereas the lower boundary of the model is the regional geothermal heat flow of 65 mW·m^{-2} representing the CAP scenarios and 110 mW·m^{-2} representing the KM, applied at a depth of 20 km beneath the upper boundary, with constant heat flux at the lower boundary and heat and fluid passage on both right and left boundaries of the model has been prevented, therefore no heat and fluid pass through either side of the model. In modelling, the topography on the surface is represented by static groundwater level and fluid inflow and outflow are considered free (Wisian and Blackwell, 2004). It is worth mentioning that it is a challenge to specify the boundaries of the water table. To overcome complexity, the water table has been specified at the top boundaries of the model. The geometry of the model is 23 km in length on x-axis and 20 km in breadth on y-axis, comprising an area of 460 km^2, basement of the model starts at a depth of d_z=-8000 m downwards of the domain. The topographic relief of H=0, 10, 100, 500, 1000, 1500 m is variable based on the scenario of model, varying the breadth and area of the model domain. In addition, the length of the model is not limited to 23 km, but for modelling purposes such a length suffices the scope of the study. The model geometry of H=500 m is in **Figure A.1**, where, also, the location of the synthetic temperature-depth vertical profile (e-profile) is visible, where the starting point is off the base of topographic relief and fault top from upper boundary in the basin to the bottom of fault, meeting the fault zone at some subsurface depth. The e-profile is produced to analyse the behaviour of temperature in the model in vertical profile, compared to a typical fault zone T-D profile. The model used in this study is a cross-section of a typical fault-controlled geothermal systems. All the final scenarios are computed to simulate for 1 Myr which is sufficient time for the system to be under steady-state conditions.

2.3.3. Parameters of model

In all models, the fault zone thickness (fz) is considered as 250 m wide. In addition, thin

impermeable layers were placed on both sides of the fault zone to represent fault sealing as 25 m wide. Parry et al. (1988); Wisian and Blackwell (2004) suggests the formation of fault walls at the margins form due to chemical precipitation. **Table 2.1** summarizes the fixed physical parameters and their values used in reference model, respectively. The following parameters was retrieved from different sources in the literature, producing a comprehensive list of parameters.

Table 2.1 Parameters used in the reference model.

Parameter: unit	**Value**	**References**
fz: m	200	(McKenna and Blackwell, 2004; Person et al., 2012; Wisian and Blackwell, 2004)
λ: $W \cdot m^{-1} \cdot K^{-1}$	2.5 (Bed rock) 1.25 (Basin-fill)	(Guillou-Frottier et al., 2013; Magri et al., 2015; Person et al., 2012)
β: K^{-1}	2.1×10^{-4}	(Bodri and Rybach, 1998; Stauffer et al., 1997)
K: m^2	Fault zone: 10^{-14} Bed rock: 10^{-16} Basin-fill: 2×10^{-16} Fault sealing zone: 10^{-18}	(Bodri and Rybach, 1998; Forster and Smith, 1988; Guillou-Frottier et al., 2013; McKenna and Blackwell, 2004; Neuzil, 1994; Person et al., 2012; Rabinowicz et al., 1998; Smith and Chapman, 1983)
T_0: °C	20	(Magri et al., 2017; Pearson-Grant and Bertrand, 2021; Person et al., 2012; Wisian and Blackwell, 2004)
ρ: $kg \cdot m^{-3}$	998.2 (20 °C)	(Smith and Chapman, 1983; Stauffer et al., 1997)
P_0: Pa	10^5	(Pearson-Grant and Bertrand, 2021)
$c\rho$: $J \cdot kg^{-1} \cdot K^{-1}$	4182	(Person et al., 2012; Stauffer et al., 1997)
σ: --	0.75	(Rabinowicz et al., 1998)

The permeabilities used in the domain are 10^{-16} m^2 and 10^{-18} m^2 based on the scenario except for the fault zone 10^{-14} m^2, fault sealing 10^{-18} m^2, and basin 2×10^{-16} or 2×10^{-18} m^2, according to the scenario of the model. In addition, the thermal conductivity of 2.5 $W \cdot m^{-1} \cdot K^{-1}$, a characteristic of basement rocks, employed homogeneously in model domain.

2.4. Model Validation

A comparison was made with the results of a study conducted by Wisian and Blackwell

(2004). In their study, a different geometric model under the geometry and boundary conditions proposed in **Figure 2.1** was used. TOUGH2, a commercial software, was used in their work, which has been developed specifically for modelling of geothermal systems and has been employed in many scientific studies for years.

As part of the validation study, the model geometry and boundary conditions used by Wisian and Blackwell (2004) were created in the FlexPDE environment. The equations mentioned in **2.3.1** has been used directly as conservation equations. Unlike Wisian and Blackwell (2004) model, base of the model was defined as an impermeable zone, K=10^{-20} m^2, and a constant basal heat flow was applied at the base, providing same temperature gradient along the bottom boundary of the model. This approach is widely employed in similar hydrological modelling studies such as the (Forster and Smith, 1988).

The model comparison results for two different bedrock permeability, K_2, are shown in **Figure B.1**, where K_1=2xK_2 for basin in all models and K_3=10^{-14} m^2 for fault zone were considered. The thermal conductivity values in bedrock, λ_1=2.5, and basin-fill, λ_2=1.25 $W \cdot m^{-1} \cdot K^{-1}$ were considered.

In the models produced by both the studies, firstly, the problem was solved under the condition of time-independent thermal conduction and hydrostatic pressure, and these results were used as the initial state in convection models. In their models, 90 $mW \cdot m^{-2}$ was used as the basal heat flow.

Evaluating the temperature distributions shown in **Figure B.1**, results of both different simulations produced similar results in regional temperature distribution. In addition, however, some differences between the models are evident. For example, at fault zone temperature, it is observed that in low permeability, K=10^{-18} m^2, the temperature value at the base of the fault zone in Wisian and Blackwell (2004) model had been calculated as approximately 180 °C and 200 °C in this study model. In high transmittance model, K=10^{-16} m^2, at the base of the fault zone in Wisian and Blackwell (2004) model had been calculated as approximately 200 °C and 225 °C in this study model. These temperature differences are likely due to differences in the definition of baseline conditions between the models.

In Wisian and Blackwell (2004) model, it was accepted that the base is insulated against fluid passage, d_z=-8000 m. While in the study model, it has been observed that there is

a very slight upward convection from the impermeable area in the base. For this reason, the fault zone temperature in the study model has been approximately 20 to 25 °C higher. On the other hand, it can be expected that these differences are at least partially related to the differences in the values of physical parameters used in solving the equations, temperature-dependent density and viscosity, heat capacities among others. Wisian and Blackwell (2004) did not provide information about these parameters in their model. As a result, the fluid simulation model developed within the scope of the project produced suitable results for modelling the topography effect in geothermal systems.

Since Wisian and Blackwell (2004) model in **Figure B.1** used in validation studies is suitable for parametric modelling of the Q_b and H values to be investigated in this study, the same model has been considered for further investigation. Six different scenarios, H=0, 10, 100, 500, 1000, 1500 m were modelled to calculate the topography effect in geothermal system formation.

2.5. Field Well Data

For CA Region, MTA geothermal inventory (Akkuş et al. 2005) was used to retrieve datasets such as the fault lines, well data and coordinates. Moreover, additional well data had been obtained from the literature (Afşin and Baş, 1997; Akbaşlı, 1992; Akıllı and Mutlu, 2018; Burçak, 2009; Çelmen, 2008; Çetin and Şimşek, 2008; Dağıstan et al., 2008; Gevrek, 2000; Gündüz and Özten, 1994; Kahraman, 2014; Kara, 2009, 2007; Karadağlar, 2013; KOP İdaresi et al., 2020; Ölmez and Gevrek, 1991; Özeke, 1987; Özen Türker, 2006; Simsek et al., 2010; Zengin, 2014). Another question that has been raised is, how the data is collected, and the techniques used in well-data temperatures. To analyse the well-data, all well-data should be of consistent techniques and methods. According to Vaught, (1980); Vieira and Hamza (2011), for temperature data obtained at various depths, linear regression is the method to define a geothermal gradient and exclude shallow wells due to the environmental effects of precipitation and groundwater flow at the subsurface. Geothermal wells deeper than d_w=-300 m are good indications of actual temperatures of the regional convection system as well-temperature data might not be affected by the shallow complex fracturing effects (Blackwell et al., 2012). In T-D profiles, complex distribution is observed between shallow and medium depths. This dispersion is related to shallow effects such as geological complexity and groundwater

flow.

A total of number of 266 geothermal wells in 37 geothermal fields were gathered within the CA Region. However, due to insufficient data reported in the literature, only 141 geothermal wells in 32 geothermal fields were considered for investigation in the study. Out of 13 provinces in CA Region, 11 provinces host geothermal sources. In Kırıkkale and Karaman provinces, geothermal resources do not exist as per the MTA inventory (Akkuş et al., 2005).

2.6. Elevation Profiles

In this study, we develop and evaluate the topographic relief (H) for geothermal systems in the CA Region. The objective is to develop a simple approach of two-dimensional elevation profiles for geothermal systems, consisting of three steps. First, a radius of approximately 5 km for a geothermal field of interest is encircled from the geothermal source shown in **Figure 1.1** using the Google Earth tools. Second, fault lines within the circle are located referring to MTA inventory (Akkuş et al., 2005), and elevation profile is delineated perpendicular to the fault line using the Google Earth tools. Replicative number of elevation profiles were delineated similarly to produce a quantifiable number of elevation profiles for the purpose of variety. Third, the elevation profile suggesting maximum elevation difference from the highest to lowest elevation was selected for the study as the following **Eq. (2.5)**:

$$\mathrm{H} = \text{highest elevation} - \text{lowest elevation} \qquad \textbf{Eq. (2.5)}$$

The encircling and delineation of a geothermal field are demonstrated in **Appendix C.**, comprehensively.

2.7. Data Challenges

Geothermal reservoirs involving hydrothermal alteration and structural heterogeneity are challenging targets (Blackwell, 1985). This is suggested due to lack of subsurface data, unexplored basement lithology and uncertain permeability as it is challenging to conduct field tests and obtain results in such environments. Since the data is limited to shallow surfaces, the investigation of hydrothermal systems and understanding of deep processes are restricted to topography, structure measurements and spring temperatures

(Belgrano et al., 2016). However, in recent times, numerical modelling of hydrothermal systems has been considered to probe the underlying mechanisms of deep processes, hot spring formation, and their controlling factors, comprehensively (Forster and Smith, 1989; López and Smith, 1995; Magri et al., 2016; Wisian and Blackwell, 2004).

2.8. Temperature Anomaly

To calculate temperature anomaly (ΔT), several quantities are undertaken to yield ΔT. Firstly, borehole log consists of two parameters of interest, the well depth (d_w) and well temperature (T_w). Although, bottom-well temperature (T_{bw}) represents the actual thermal condition of the geothermal well, however, almost all the borehole-logs have included measurement of well-head temperature (T_{wh}), and or measurement method has not been mentioned, in this study, T_w was considered as temperature measured along any depth of the well. Proceeding, conductive background temperature (T_b) is interpolated using subsurface conductive temperature profiles. Interpolation was employed based on d_w of each well and Q_b of CAP and KM separately. Followed by the yield of ΔT as the above-mentioned two quantities were employed in the below **Eq. (2.6)**:

$$\Delta T = T_w - T_b \qquad \textbf{Eq. (2.6)}$$

Some studies calculate geothermal gradient employing T_{bw}, as a necessity to produce T-D profiles, however, due to insufficient data in borehole logs of the CA Region, in this study, ΔT was considered.

Subsequently, the maximum temperature-depth graph has been plotted in relationship to maximum temperature anomaly on y-axis and well depth on x-axis for the existing wells that represent the maximum temperature anomaly in d_w=-300 m in the specific geothermal field. Usually, at a geothermal field, more than one borehole is drilled due to technical deficiencies in obtaining reliable borehole data. To obtain borehole data, various measurement methods are available in literature, and a range of techniques are adopted, imposing challenge to yield consistent geothermal gradient and temperature anomalies, leading to undesirable outcomes. To overcome the challenge, the average temperature anomaly had been introduced to decrease the discrepancy of borehole data. In that respect, the average temperature-depth graph has been plotted in relationship to average temperature anomaly on y-axis and well depth on x-axis for the existing wells

that represent the maximum temperature anomaly in d_w=-300 m in specific geothermal field. For both maximum and average temperature anomaly graphs, only geothermal fields that consist of d_w=-300 m and below were considered for study comparison.

3. RESULTS AND DISCUSSION

Within the scope of numerical modelling, convection models were developed for different values of topographic relief (H) and basal heat flow (Q_b). A total of 26 scenarios were produced to study for K=10^{-16} m^2. In addition, the scenarios for K=10^{-18} m^2 were produced in this study, however, the T-D profiles and Nusselt number (Nu) graph are not included in the study, as no significant convection was observed in the scenarios produced. In this study, T-D profiles along the fault zone, T-D of e-profile, Nu graph and comparison of the produced study model (reference model) with the CA Region geothermal fields are investigated. The Temperature-depth along fault zone and along vertical profiles were produced to investigate the fluid temperatures in the geothermal resources. profiles demonstrated differences in fluid temperature as the basal heat flow and topographic relief changes.

3.1 Fault Zone

Fault zone temperatures in the produced convection models are in **Figure 3.1**. Panel a) shows the temperatures along the fault zone where the heat flow (Q_b) is 110 $mW \cdot m^{-2}$ and Panel b) shows the temperatures along the fault zone where the heat flow (Q_b) is 65 $mW \cdot m^{-2}$. To understand the effect of topography, different models were produced using H=0, 10, 100, 500, 1000 and 1500 m. The average H in all 32 geothermal fields in CA Region is of approximately 1050 m. In **Figure 3.1**, black dashed curves show initial temperature of the fault, and the coloured curves show the fault temperature when the geothermal system is formed.

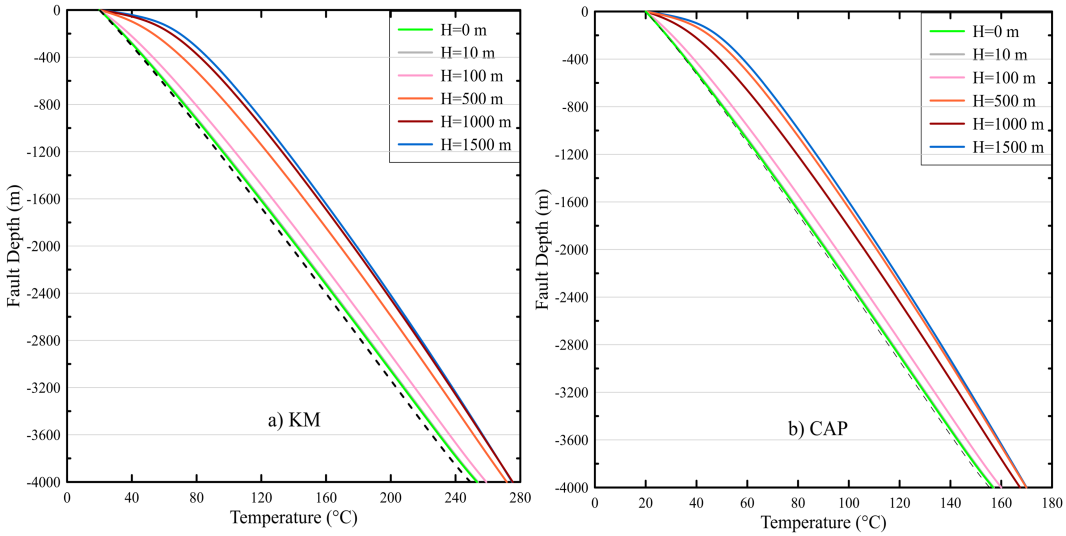

Figure 3.1 Temperatures obtained along the fault zone for H values in a) KM and b) CAP.

As can be seen in **Figure 3.1**, temperature increase in the fault zone increases due to both the heat flow and topography. In addition, in cases where the topography is low, H lower than 100 m, it is observed that the temperature increase in the fault zone is low. This is evident in topography as a significant effect on natural convection. On the other hand, as topography increases, the increase in fault zone temperatures become less effective. The temperature scenario of H=500 is in **Figure A.3**.

3.2 Vertical Profile

To calculate the effect of convection on a synthetic vertical borehole, depth of dz=-4000 m was selected, and position of the profile is indicated by the letter "e" in **Figure A.1**. The results obtained are shown in **Figure 3.2** for different H and Q_b values. Borehole meets the fault at approximately dz=-2000 m in **Figure 3.2**. While a significant increase in temperatures is observed in the parts above the fault zone depending on the top fault, not much difference in temperatures is observed after crossing the fault zone. Comparing T-D e-profile of a) Q_b=110 mW·m^{-2} and b) Q_b=65 mW·m^{-2} in **Figure 3.2** demonstrates that each basal heat flow yields quite different results.

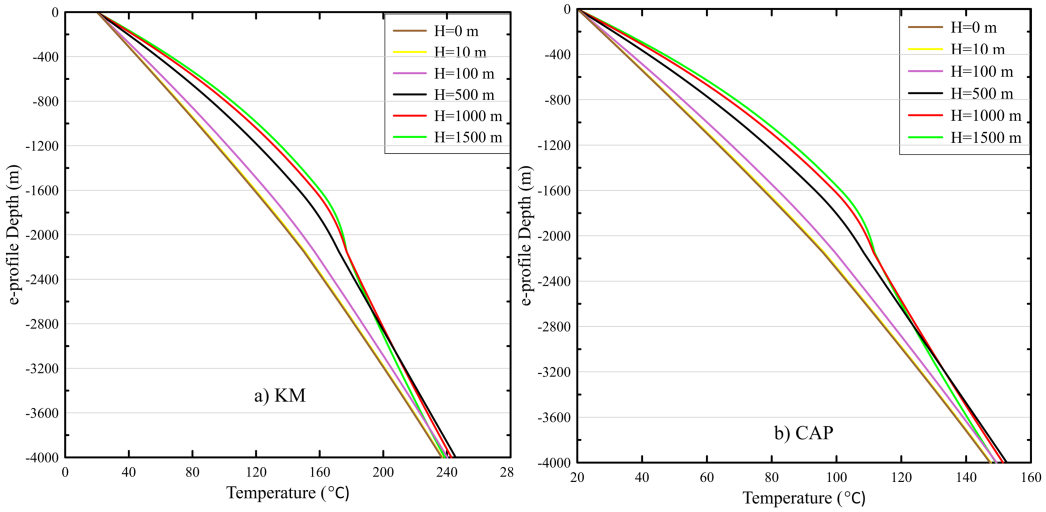

Figure 3.2 T-D curves of e-profile meeting fault zone in a) KM and b) CAP.

3.3 Nusselt Number

To examine the total energy output of transport-based system of the topography effect, the Nusselt number (Nu) was calculated for different H and Q_b scenarios. This number allows us to calculate the magnitude of the convectional energy transfer in the system according to conduction-based energy transfer, Nu=1 indicates that energy transfer is entirely by the thermal conduction (Nield and Bejan, 2006). For this purpose, after the surface heat flow values of the initial and final state for each scenario was calculated along the topographic surface, integrated along the surface to get what is called as the "heat loss". Then, final heat loss value in the scenarios was divided by initial heat loss value. The results are in **Figure 3.3** for all the H and Q_b scenarios.

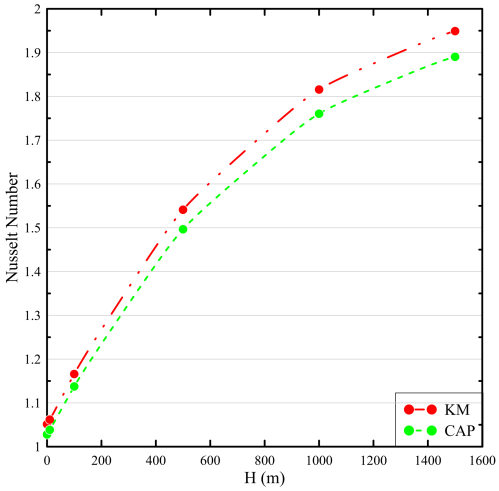

Figure 3.3 Nusselt number (Nu) values calculated for different H and Q_b scenarios in KM and CAP.

The Nusselt number rate of increase starts to decrease above H=1000 m. Accordingly, the Nu value increases in proportion to the topography. This is because, with the increase in topography, the circulation depth increases, and more thermal energy is transferred to the surface by convection.

3.4 Field Well Data-Reference Model Comparison

To compare the relationship between fault zone temperatures and topography obtained in this study with the temperatures measured in the geothermal fields in the CA Region, T-D measurements of 141 geothermal boreholes in 32 geothermal fields were gathered. As a data source, firstly, MTA geothermal inventory (Akkuş et al., 2005) was referred. However, if any T-D measurements conducted in the geothermal fields in the following years came into existence in updates or discoveries, then these were retrieved from the literature and added into this study. In the comparison, temperature values measured at points of d_w-=-300 m or deeper were used to minimize geological effects close to the surface.

T-D measurements usually conducted by different methods at any geothermal field are available in the literature. Among the measured temperatures in well, the most reliable representation of natural geothermal temperatures is the T_{bw}. However, this information is sometimes unclear in the literature. The geothermal system temperatures are usually reported as maximum temperature value measured in the geothermal field. On the other hand, due to the uncertainties given above, average temperature values measured in the field were also used for the comparison. In **Figure 3.4**, the temperature anomaly was calculated to compare the outcome results produced by the reference model against the temperatures measured in the geothermal fields.

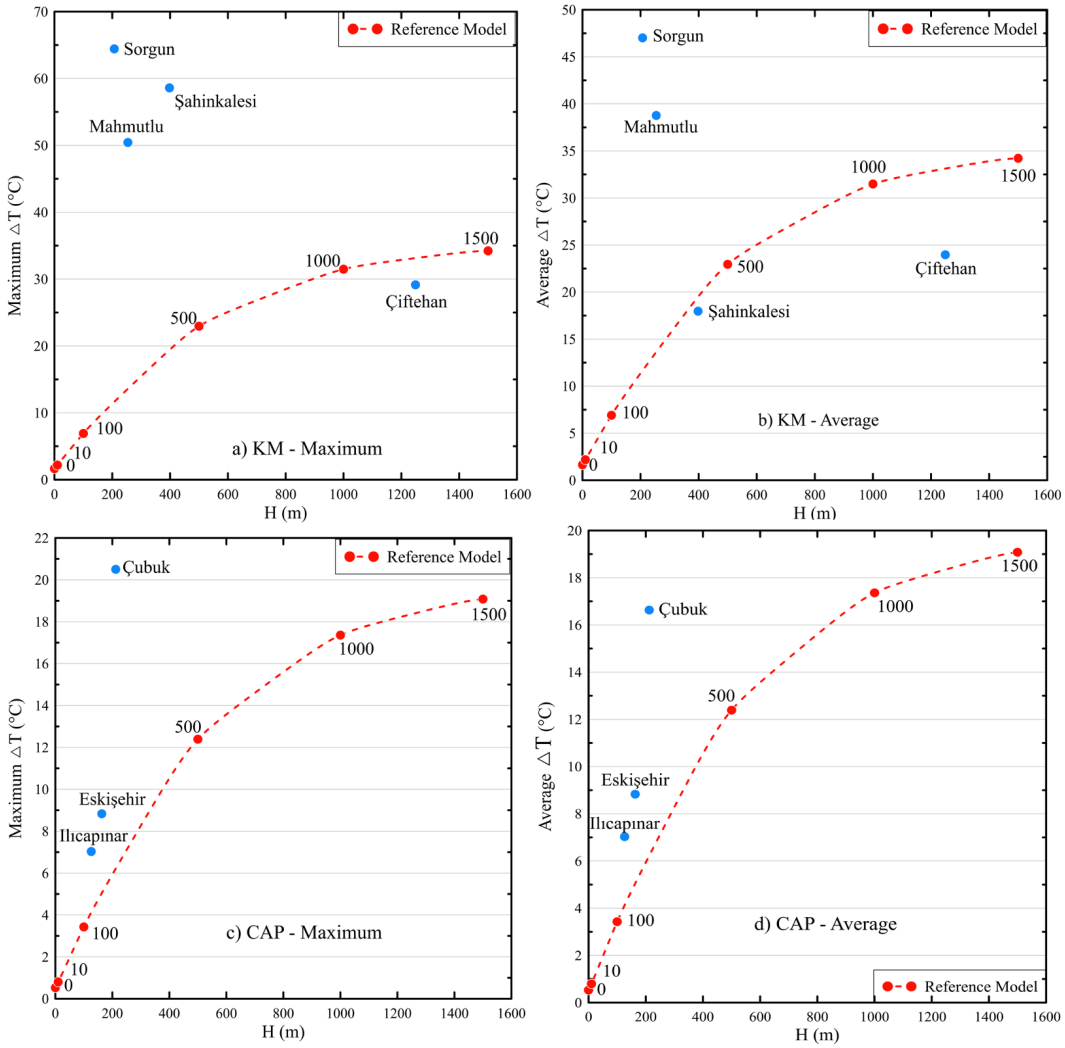

Figure 3.4 Comparison of temperature anomalies of the fault zone calculated in the reference models and temperature anomalies measured in the geothermal fields of the CA Region.

The calculation method for temperature anomaly is discussed in this study. In **Figure 3.4**, a) and b) demonstrate geothermal fields in KM, whereas c) and d) demonstrate the geothermal fields in CAP. Also, a) and c) were obtained based on maximum temperature anomalies, b) and d) were obtained based on average temperature anomalies measured in the geothermal fields. For the temperature anomalies measured in the fields, the static crustal temperature value in the region was taken as a reference. The crustal thermal model used by Balkan-Pazvantoğlu and Erkan (2019) was used to calculate the regional crustal temperature. The changes of the temperature anomaly values obtained from the numerical models and measured in the fields according to the topographic relief (H) are illustrated in **Figure 3.4**. The first result that stands out in **Figure 3.4** is the numerical model and temperature anomaly values measured at geothermal fields in blue dots are

generally compatible. This result shows that the regional permeability value used in the model represents the regional permeability value in these fields in general terms.

When the temperature anomaly values measured at geothermal fields were compared with the reference model in red curve, higher temperatures were measured in some sites compared to those calculated from the models, while lower temperatures were measured in some geothermal fields. In particular, the temperatures measured in the geothermal fields in KM are significantly higher. Numerical models show that natural convection is strongly effective, and the topographic effect decreases with the increasing regional permeability (Wisian and Blackwell, 2004). In addition, since heat flow (Q_b) is high in KM (Balkan-Pazvantoğlu and Erkan, 2019), a suitable condition for natural convection is created. As high permeability, K=10^{-15} m^2 values was used, convection occurs along the fault zone even in the absence of topography. In this study, it was calculated that as low permeability, K=10^{-16} m^2 was used, the topography effect was also evident when there is high basal heat flow (Q_b) in **Figure 3.2** and **Figure 3.3**. In cases where the permeability is higher, the natural convection can be expected to be more effective. As a result, higher permeability may be effective in areas where high temperatures are observed in Sorgun, Şahinkalesi and Mahmutlu geothermal fields. Even if the regional permeability is not high in these geothermal fields, the permeability may be high with cracks at the depths where the measurements are made, and this may provide upward convection of the hot geothermal fluid by natural convection (Erkan et al., 2008).

Furthermore, the effect of topography on the geothermal systems in the CA Region has been emphasized in various field-based studies. For example, in a study conducted by Yurteri and Simsek (2017) in Savcılı geothermal field located within the boundaries of KM, oxygen isotope measurements showed that the geothermal source was of meteoric origin, analysed along with water chemistry analyses and modelled that the geothermal source was fed from the hills located in northeast of the field and approximately 500 m above the hot spring. The source temperature of the geothermal field was measured according to the silica geothermometer, ranging from 68 to 74 °C. According to model results obtained from the current study in **Figure 3.4** a) and b), source circulation depth corresponds to ~1 km for a difference of 27 °C (assuming regional geothermal gradient value as 40 °C·km^{-1}), which is in agreement with the circulation model proposed here. As a result, it is observed that the topography effect, forced convection, dominates the

convection in the Savcılı geothermal field. A similar study was conducted by Şener and Baba (2019) in the Kozaklı (Nevşehir) geothermal field, where geothermal fluid was shown to be of meteoric origin by the geochemical measurements. Moreover, in a study conducted by Afsin et al. (2014) in some geothermal fields in the Cappadocia region with fluid chemistry analyses, it was shown that the geothermal system in all systems is of meteoric origin and the effect of topography on cycle mechanism was emphasized. On the other hand, the fact that the chemical values measured in these areas are almost unrelated to the seasonal precipitation shows that the circulation takes place at deep levels. If a waterbody is in the vicinity of geothermal systems, dynamics of groundwater changes, leading to variable fluid deep circulation, to some degree (Frisbee et al., 2013, 2017).

4. CONCLUSION

According to the results obtained from the numerical simulations, it is observed that topography has a significant effect on the fault zone temperatures in the geothermal systems, in general. Although constant fault depth was used in all models, higher fluid temperatures were calculated with the increase in topography along the fault zone. If the heat flow is high, the heating in the fault zone is higher. It was observed that the well temperature measurements in the geothermal fields in the CAP were compatible with the model results.

The results of this study revealed the relationship between the reservoir temperatures, topography, and the heat flow in geothermal systems under ideal conditions with the numerical simulations. In these simulations, medium permeability and fault zone depth were considered as constant. Although the feasibility of a geothermal system depends on fluid efficiency (flow rate), as well as source temperature, effect of topography and heat flow on convective energy transfer and source temperature were examined in this study. Considering permeability can be increased with the aid of fracking technologies, as it is the case with Enhanced Geothermal Systems (EGS) (Chandrasekharam et al., 2023; Chandrasekharam and Baba, 2021), it is possible to conclude that the topography and heat flow influences the geothermal system temperature increasing the production potential of the geothermal system.

The fault zone temperatures obtained according to different topographic conditions calculated in this study give the temperatures to be obtained in a geothermal system forced by the topography effect in an area. According to the results obtained from the models, it is possible to calculate the expected geothermal temperatures in a region under the influence of topography, depending on the heat flow. On the other hand, while the H affects the circulation depth quite a lot at low values, its effect decreases at geothermal temperatures when it is higher, H >~1000 m. The higher the H, the larger fluid circulation. As evident from the numerical results, the driving factor in controlling the hot spring locations and the fluid pathways of CA Region hydrothermal systems is dominated by topography.

Under idealized geological conditions, such as homogeneous bedrock properties and single main fault zone, this study investigated the effect of topographic relief and heat flow on fault zone temperatures. However, these simplified assumptions may not be valid for a particular geothermal field and the geological and structural features of the site may need to be considered. For example, with a low permeability upper zone, such as a "cap rock", as observed in many geothermal fields, a desirable stable geothermal system can be formed even if the bedrock permeability is very high. On the other hand, since the main fault zone is more fractured near the surface, higher temperatures than predicted by the simulations can be obtained on the fault zone because of thermal convection. These situations have been observed in many geothermal systems in CA and elsewhere.

Deeper boreholes are to be drilled and geothermal gradients are to be measured based on topographic influence and features in smaller spatial scales rather than larger spatial scales. Thus, it is important to investigate geothermal gradients based on topographic relief in smaller spatial scales for future studies.

REFERENCES

Afsin, M., Allen, D.M., Kirste, D., Durukan, U.G., Gurel, A., Oruc, O., 2014. Mixing processes in hydrothermal spring systems and implications for interpreting geochemical data: A case study in the Cappadocia region of Turkey. Hydrogeol J 22, 7–23. https://doi.org/10.1007/s10040-013-1056-2

Afşin, M., Baş, H., 1997. Bazı önemli soğuk ve sıcak su kaynaklarının hidrokimyasal ve izotopik incelemesi ve kökensel yorumu (Aksaray-Niğde arası). TÜBİTAK numaralı proje 64, TÜBİTAK.

Akbaşlı, A., 1992. Niğde-Sofular-Acıgöl sıcak su sondajları (NAR-1, MTA-1,2,3,4) kuyu bitirme raporu. Maden Tetkik ve Arama Genel Müdürlüğü Report No.: 9407. Ankara.

Akıllı, H., Mutlu, H., 2018. Polatlı ve Haymana (Ankara) sıcak sularının kökenine yönelik kimyasal ve izotopik sınırlamalar. Hacettepe Üniversitesi Yerbilimleri Uygulama ve Araştırma Merkezi Bülteni 39, 41–64.

Akkuş, İ., Akıllı, H., Ceyhan, S., Dilemre, A., Tekin, Z., 2005. Türkiye Jeotermal Kaynaklar Envanteri. Maden Tetkik ve Arama Genel Müdürlüğü Envanter Serisi-201. Maden Tetkik ve Arama Genel Müdürlüğü, Ankara.

Altın, T.B., Barak, B., Altın, B.N., 2012. Change in Precipitation and Temperature Amounts over Three Decades in Central Anatolia, Turkey. Atmospheric and Climate Sciences 02, 107–125. https://doi.org/10.4236/acs.2012.21013

Anderson, S.P., Dietrich, W.E., Montgomery, D.R., Torres, R., Conrad, M.E., Loague, K., 1997. Subsurface flow paths in a steep, unchanneled catchment. Water Resour Res 33, 2637–2653. https://doi.org/10.1029/97WR02595

Aydar, A., Gündoğdu, N., Bayhan, H., Gourgaud, A., 1994. Kapadokya Bölge'sinin Kuvaterner yaşlı volkanizmasının volkanik-yapısal ve petrolojik incelemesi. TÜBİTAK Yerbilimleri Dergisi 3, 25–42.

Aydar, E., Çubukçu, H.E., Şen, E., Akin, L., 2013. Central Anatolian Plateau, Turkey: Incision and paleoaltimetry recorded from volcanic rocks. Turkish Journal of Earth Sciences 22, 739–746. https://doi.org/10.3906/yer-1211-8

Balkan-Pazvantoğlu, E., Erkan, K., 2019. Temperature-depth curves and heat flow in central part of Anatolia, Turkey. Tectonophysics 757, 24–34. https://doi.org/10.1016/j.tecto.2019.02.019

Ball, L.B., Caine, J.S., Ge, S., 2014. Controls on groundwater flow in a semiarid folded and faulted intermountain basin. Water Resour Res 50, 6788–6809. https://doi.org/10.1002/2013WR014451

Barka, A., Reilinger, R., 1997. Active tectonics of the Eastern Mediterranean region: deduced from GPS, neotectonic and seismicity data. Annali Di Geofisica 11.

Belgrano, T.M., Herwegh, M., Berger, A., 2016. Inherited structural controls on fault geometry, architecture and hydrothermal activity: an example from Grimsel Pass, Switzerland. Swiss J Geosci 109, 345–364. https://doi.org/10.1007/s00015-016-0212-9

Blackwell, D.D., 1985. A transient model of the geothermal system of the Long Valley Caldera, California. J Geophys Res Solid Earth 90, 11229–11241. https://doi.org/10.1029/JB090iB13p11229

Blackwell, D.D., Waibel, A.F., Ricards, M., 2012. Why Basin and Range Systems are hard to find: The moral of the story is they get smaller with depth! GRC Transactions 36, 1321–1326.

Bodri, B., Rybach, L., 1998. Influence of topographically driven convection on heat flow in the Swiss Alps: a model study. Tectonophysics 291, 19–27.

Burçak, M., 2009. Water chemistry and isotope studies in Aksaray geothermal fields (Acıgöl-Ziga-Şahinkalesi), Central Anatolia, Turkey. Bulletin of the Mineral Research and Exploration 138, 45–68.

Çelmen, O., 2008. Sivrihisar ve Beypazarı bölgesinde yeralan sıcak ve mineralli su kaynaklarının hidrojeokimyasal ve izotopik incelenmesi (Doktora tezi). Ankara Üniversitesi, Fen Bilimleri Enstitüsü, Ankara.

Çetin, A., Şimşek, Ş., 2008. Karakaya ve Ilıcaköy Ayaş (Ankara) sıcak sularının hidrojeoloji incelemesi. Mühendislik Jeoloji Bülteni 0, 67–80.

Chandrasekharam, D., Baba, A., 2021. High heat generating granites of Kestanbol: Future enhanced Geothermal System (EGS) province in western Anatolia. Turkish Journal of Earth Sciences 30, 1032–1044. https://doi.org/10.3906/yer-2106-16

Chandrasekharam, D., Singh, M., Baba, A., 2023. Sahinkalesi massif, a resurgent dome and super-hot EGS province: Hasandag stratovolcanic province, Central Anatolia, Renewable Energy.

Cosentino, D., Schildgen, T.F., Cipollari, P., Faranda, C., Gliozzi, E., Hudáčková, N., Lucifora, S., Strecker, M.R., 2012. Late Miocene surface uplift of the southern margin of the Central Anatolian plateau, Central Taurides, Turkey. Bulletin of the Geological Society of America 124, 133–145. https://doi.org/10.1130/B30466.1

Craw, D., Upton, P., Horton, T., Williams, J., 2013. Migration of hydrothermal systems in an evolving collisional orogen, New Zealand. Miner Depos 48, 233–248. https://doi.org/10.1007/s00126-012-0421-8

Dağıstan, H., Kara, İ., Duru, M., 2008. Nevşehir-Kozaklı jeotermal sahasında yeni bulgular, in: Termal ve Maden Suları Konferansı.

Dewey, J.F., Pitman III, W.C., Ryan, W.B.F., Bonnin, J., 1973. Plate tectonics and the Evolution of the Alpine System. Geol Soc Am Bull 84, 3137–3180. https://doi.org/10.1130/0016-7606(1973)84<3137:PTATEO>2.0.CO;2

Erdogmus, B., Toksoy, M., Ozerdem, B., Aksoy, N., 2006. Economic assessment of geothermal district heating systems: A case study of Balcova-Narlidere, Turkey. Energy Build 38, 1053–1059. https://doi.org/10.1016/j.enbuild.2006.01.001

Erkan, K., Holdmann, G., Benoit, W., Blackwell, D., 2008. Understanding the Chena Hot Springs, Alaska, geothermal system using temperature and pressure data from exploration boreholes. Geothermics 37, 565–585. https://doi.org/10.1016/j.geothermics.2008.09.001

ETKB, 2021. https://enerji.gov.tr/eigm-yenilenebilir-enerji-kaynaklar-jeotermal [WWW Document]. Republic of Türkiye, Ministry of Energy and Natural Resources.

Faulds, J., Coolbaugh, M., Bouchot, V., Moeck, I., Oğuz, K., 2010. Characterizing structural controls of geothermal reservoirs in the Great Basin, USA, and Western Turkey: Developing successful exploration strategies in extended terranes, in: World Geothermal Congress 2010. Bali, Indonesia.

Faulds, J.E., Bouchot, V., Moeck, I., Oğuz, K., 2009. Structural controls on geothermal systems in Western Turkey: A preliminary report, in: GRC Transactions. p. 375.

Feth, J.H., 1964. Hidden Recharge. https://doi.org/https://doi.org/10.1111/j.1745-6584.1964.tb01780.x

Fetter, C.W., 2011. Applied Hydrogeology, 4th ed. Prentice Hall, Upper Saddle River.

Forster, C., Smith, L., 1989. The influence of groundwater flow on thermal regimes in mountainous terrain: A model study. J Geophys Res 94, 9439–9451. https://doi.org/10.1029/JB094iB07p09439

Forster, C., Smith, L., 1988. Groundwater flow systems in mountainous terrain 1. numerical modeling Technique. Water Resour Res 24, 999–1010.

Frisbee, M.D., Phillips, F.M., White, A.F., Campbell, A.R., Liu, F., 2013. Effect of source integration on the geochemical fluxes from springs. Applied Geochemistry 28, 32–54. https://doi.org/10.1016/j.apgeochem.2012.08.028

Frisbee, M.D., Tolley, D.G., Wilson, J.L., 2017. Field estimates of groundwater circulation depths in two mountainous watersheds in the western U.S. and the

effect of deep circulation on solute concentrations in streamflow. Water Resour Res 53, 2693–2715. https://doi.org/10.1002/2016WR019553

Gascoyne, M., Sheppard, M.I., 1993. Evidence of Terrestrial Discharge of Deep Groundwater on the Canadian Shield from Helium in Soil Gases. Environ. Scl. Technol 27, 2420–2428.

Gevrek, A.I., 2000. Water/rock interaction in the Kızılcahamam Geothermal Field, Galatian Volcanic Province (Turkey): a modelling study of a geothermal system for reinjection well locations. Journal of Volcanology and Geothermal Research 96, 207–213.

Görür, N., Oktay, F.Y., Seymen, I., Şengör, A.M.C., 1984. Palaeotectonic evolution of the Tuzgölü basin complex, Central Turkey: sedimentary record of a Neo-Tethyan closure. Geol Soc Spec Publ. https://doi.org/10.1144/GSL.SP.1984.017.01.34

Guillou-Frottier, L., Carre, C., Bourgine, B., Bouchot, V., Genter, A., 2013. Structure of hydrothermal convection in the Upper Rhine Graben as inferred from corrected temperature data and basin-scale numerical models. Journal of Volcanology and Geothermal Research 256, 29–49. https://doi.org/10.1016/j.jvolgeores.2013.02.008

Gündüz, M., Özten, A., 1994. Yozgat-Yerköy Güven kaplıcası sıcaksu sondajı YK-1 kuyu bitirme ve koruma alanları raporu. MTA Genel Müdürlüğü Enerji Hammadde Etüt ve Arama Dairesi Başkanlığı, Rapor No.: 9796. Ankara.

Hepbasli, A., Ozgener, L., 2004. Development of geothermal energy utilization in Turkey: A review. Renewable and Sustainable Energy Reviews 8, 433–460. https://doi.org/10.1016/j.rser.2003.12.004

Hoogland, O., Veenstra, E., Opinska, L.G., Vega, P.T., Rademaekers, K., 2019. Study on impacts of EU actions supporting the development of renewable energy technologies. Luxembourg.

Igliński, B., Pietrzak, M.B., Kiełkowska, U., Skrzatek, M., Gajdos, A., Zyadin, A., Natarajan, K., 2022. How to Meet the Green Deal Objectives—Is It Possible to Obtain 100% RES at the Regional Level in the EU? Energies (Basel) 15. https://doi.org/10.3390/en15062296

İlbeyli, N., Pearce, J.A., Thirlwall, M.F., Mitchell, J.G., 2004. Petrogenesis of collision-related plutonics in Central Anatolia, Turkey. Lithos 72, 163–182. https://doi.org/10.1016/j.lithos.2003.10.001

Kahraman, S., 2014. Investigation of the Geothermal System of Kızılinler Eskişehir (Master's Thesis). Anadolu University, Graduate School of Sciences, Eskişehir.

Kara, İ., 2009. Nevşehir Kozaklı MTA-K4 jeotermal araştırma sondajı kuyu bitirme raporu. Derleme. Maden Tetkik ve Arama Genel Müdürlüğü Rapor: 11182. Ankara.

Kara, İ., 2007. Aksaray-Güzelyurt-Şahinkalesi SHK-1 sıcak su sondajı kuyu bitirme. Maden Tetkik ve Arama Rapor No.: 11004. Ankara.

Karadağlar, M., 2013. MTA Genel Müdürlüğü 2012 yılı jeotermal enerji aramaları. Maden Tetkik ve Arama Genel Müdürlüğü. Ankara.

Karlsdottir, M.R., Heinonen, J., Palsson, H., Palsson, O.P., 2020. High-temperature geothermal utilization in the context of european energy policy-implications and limitations. Energies (Basel) 13. https://doi.org/10.3390/en13123187

Kazancı, N., 2012. Geological Background and Three Vulnerable Geosites of the Kızılcahamam-Çamlıdere Geopark Project in Ankara, Turkey. Geoheritage 4, 249–261. https://doi.org/10.1007/s12371-012-0064-2

KOP İdaresi, Davraz, A., Öztürk, H.H., Nalbantçılar, M.T., Şen, F., Kozan, H., Çarıkcı, B., Sefa, M., Mermer, K., Pınarkara, Ş.Y., Toprak, A.S., Eymir, S., Güzel, T., Kalem, H., 2020. Jeotermal Kaynakların Değerlendirilmesi Projesi.

Limberger, J., Boxem, T., Pluymaekers, M., Bruhn, D., Manzella, A., Calcagno, P., Beekman, F., Cloetingh, S., van Wees, J.D., 2018. Geothermal energy in deep aquifers: A global assessment of the resource base for direct heat utilization. Renewable and Sustainable Energy Reviews 82, 961–975. https://doi.org/10.1016/j.rser.2017.09.084

López, L.D., Smith, L., 1995. Fluid flow in fault zones: Analysis of the interplay of convective circulation and topographically driven groundwater flow. Water Resour Res 31, 1489–11503.

Magri, F., Cacace, M., Fischer, T., Kolditz, O., Wang, W., Watanabe, N., 2017. Thermal convection of viscous fluids in a faulted system: 3D benchmark for numerical codes. Energy Procedia 125, 310–317. https://doi.org/10.1016/j.egypro.2017.08.204

Magri, F., Inbar, N., Siebert, C., Rosenthal, E., Guttman, J., Möller, P., 2015. Transient simulations of large-scale hydrogeological processes causing temperature and salinity anomalies in the Tiberias Basin. J Hydrol (Amst) 520, 342–355. https://doi.org/10.1016/j.jhydrol.2014.11.055

Magri, F., Möller, S., Inbar, N., Möller, P., Raggad, M., Rödiger, T., Rosenthal, E., Siebert, C., 2016. 2D and 3D coexisting modes of thermal convection in fractured hydrothermal systems - Implications for transboundary flow in the Lower Yarmouk Gorge. Mar Pet Geol 78, 750–758. https://doi.org/10.1016/j.marpetgeo.2016.10.002

Manning, C.E., Ingebritsen, S.E., 1999. Permeability of the continental crust: Implications of geothermal data and metamorphic systems. Reviews of Geophysics 37, 127–150. https://doi.org/10.1029/1998RG900002

Mayo, A.L., Morris, T.H., Peltier, S., Petersen, E.C., Payne, K., Holman, L.S., Tingey, D., Fogel, T., Black, B.J., Gibbs, T.D., 2003. Active and inactive groundwater flow systems: Evidence from a stratified, mountainous terrain. GSA Bulletin 115, 1456–1472.

McKenna, J.R., Blackwell, D.D., 2004. Numerical modeling of transient Basin and Range extensional geothermal systems. Geothermics 33, 457–476. https://doi.org/10.1016/j.geothermics.2003.10.001

McKenzie, D., 1972. Active Tectonics of the Mediterranean Region. Geophysical Journal of the Royal Astronomical Society 30, 109–185. https://doi.org/10.1111/j.1365-246X.1972.tb02351.x

Miłek, D., Nowak, P., Latosińska, J., 2022. The Development of Renewable Energy Sources in the European Union in the Light of the European Green Deal. Energies (Basel) 15. https://doi.org/10.3390/en15155576

Mock, J.E., Tester, J.W., Wright, P.M., 1997. Geothermal energy from the Earth: Its potential impact as an environmentally sustainable resource. Annual Review of Energy and the Environment 22, 305–356. https://doi.org/https://doi.org/10.1146/annurev.energy.22.1.305

Mutlu, H., 1998. Chemical geothermometry and fluid-mineral equilibria for the Ömer-Gecek thermal waters, Afyon area, Turkey. Journal of Volcanology and Geothermal Research 80, 303–321.

Neuzil, C.E., 1994. How permeable are clays and shales? Water Resour Res 30, 145–150.

Nield, D.A., Bejan, A., 2006. Convection in Porous Media. Springer, New York. https://doi.org/https://doi.org/10.1007/0-387-33431-9

Ölmez, E., Gevrek, A.İ., 1991. Aksaray-Sofular-1 (SFG1) ve Sofular-2 (SFG2) ile Ziga-Belisırma 1-2 (ZBG1 ve ZBG2) gradyan sondajları kuyu bitirme raporu. Maden Tetkik ve Arama Genel Müdürlüğü Report No.: 9194 (unpublished). Ankara.

Özeke, H., 1987. Ankara ili Ayaş ilçesi Karakaya kaplıcası AKİ ve AK2 sondajları kuyu bitirme raporu. Maden Tetkik ve Arama Genel Müdürlüğü Report No.: 8195 (Unpublished).

Özen Türker, H., 2006. Hydrogeochemical investigation of thermal and mineral waters of Sarıkaya (Yozgat) (Master's Thesis). Hacettepe Üniversitesi, Lisansüstü Eğitim-Öğretim ve Sınav Yönetmeliğinin, Ankara.

Parlaktuna, M., Mertoglu, O., Simsek, S., Paksoy, H., Basarir, N., 2013. Geothermal Country Update Report of Turkey (2010-2013), in: European Geothermal Congress 2013. Pisa, Italy.

Parry, W.T., Wilson, P.N., Bruhn, R.L., 1988. Pore-fluid chemistry and chemical reactions on the Wasatch normal fault, Utah. Geochim Cosmochim Acta 52, 2053–2063.

Pasvanoğlu, S., Çelik, M., 2018. A conceptual model for groundwater flow and geochemical evolution of thermal fluids at the Kızılcahamam geothermal area, Galatian volcanic Province. Geothermics 71, 88–107. https://doi.org/10.1016/j.geothermics.2017.08.012

PDE Solutions Inc, 2023. FlexPDE [WWW Document]. URL https://www.pdesolutions.com/index.html (accessed 1.11.22).

Pearson-Grant, S.C., Bertrand, E.A., 2021. Topography as a Major Influence on Geothermal Circulation in the Taupo Volcanic Zone, New Zealand. Geophys Res Lett 48. https://doi.org/10.1029/2020GL092248

Person, M., Hofstra, A., Sweetkind, D., Stone, W., Cohen, D., Gable, C.W., Banerjee, A., 2012. Analytical and numerical models of hydrothermal fluid flow at fault intersections. Geofluids 12, 312–326. https://doi.org/10.1111/gfl.12002

Rabinowicz, M., Boulègue, J., Genthon, P., 1998. Two- and three-dimensional modeling of hydrothermal convection in the sedimented Middle Valley segment, Juan de Fuca Ridge. J Geophys Res Solid Earth 103, 24045–24065. https://doi.org/10.1029/98jb01484

Reilinger, R., McClusky, S., Vernant, P., Lawrence, S., Ergintav, S., Cakmak, R., Ozener, H., Kadirov, F., Guliev, I., Stepanyan, R., Nadariya, M., Hahubia, G.,

Mahmoud, S., Sakr, K., ArRajehi, A., Paradissis, D., Al-Aydrus, A., Prilepin, M., Guseva, T., Evren, E., Dmitrotsa, A., Filikov, S. V., Gomez, F., Al-Ghazzi, R., Karam, G., 2006. GPS constraints on continental deformation in the Africa-Arabia-Eurasia continental collision zone and implications for the dynamics of plate interactions. J Geophys Res Solid Earth 111. https://doi.org/10.1029/2005JB004051

Reilinger, R.E., McClusky, S.C., Oral, M.B., King, R.W., Toksoz, M.N., Barka, A.A., Kinik, I., Lenk, O., Sanli, I., 1997. Global Positioning System measurements of present-day crustal movements in the Arabia-Africa-Eurasia plate collision zone. J Geophys Res Solid Earth 102, 9983–9999. https://doi.org/10.1029/96jb03736

Rempe, D.M., Dietrich, W.E., 2014. A bottom-up control on fresh-bedrock topography under landscapes. Proc Natl Acad Sci U S A 111, 6576–6581. https://doi.org/10.1073/pnas.1404763111

Şener, M.F., Baba, A., 2019. Geochemical and hydrogeochemical characteristics and evolution of Kozaklı geothermal fluids, Central Anatolia, Turkey. Geothermics 80, 69–77. https://doi.org/10.1016/j.geothermics.2019.02.012

Şener, M.F., Öztürk, M.Z., Baba, A., 2023. A review of the geothermal system evolution and distribution in the Central Anatolian Crystalline Complex (Türkiye). Turkish Journal of Earth Sciences 32, 703–720. https://doi.org/10.55730/1300-0985.1870

Şengör, A.M.C., 1980. Türkiyenin Neotektoniginin Esaslary. Geological Society of Turkey.

Şengör, A.M.C., Yılmaz, Y., 1981. Tethyan Evolution of Turkey: a plate tectonic approach. Tectonophyiscs 75, 181–241.

Serpen, U., Aksoy, N., Öngür, T., Korkmaz, E.D., 2009. Geothermal energy in Turkey: 2008 update. Geothermics 38, 227–237. https://doi.org/10.1016/j.geothermics.2009.01.002

Şimşek, S., 2009. New wide development of geothermal power production in Turkey, in: International Geothermal Days Slovakia. Častá - Papiernička, Slovakia, p. 8.

Simsek, S., Yilmaz, E., Koc, K., Turker, O., Karakus, H., Bakir, N., Gulgor, A., Simsek, Z.N., Bulus, G., Girbalar, E., Bektas, I., Savaci, T., Oguz, H., 2010. Geothermal Exploration Survey of Sorgun Geothermal Field (Yozgat-Turkey), in: Proceedings World Geothermal Congress. Bali, Indonesia, pp. 25–29.

Smith, L., Chapman, D.S., 1983. On the thermal effects of groundwater flow, 1. Regional scale systems. J Geophys Res 88, 593–608. https://doi.org/10.1029/JB088iB01p00593

Söğüt, A.R., Güzel, A., Zedef, V., Bayram, A.F., 2010. Some geological and hydrogeochemical characteristics of geothermal fields of Turkey. Scientific Research and Essays 5, 3147–3151.

St Clair, J., Moon, S., Holbrook, W.S., Perron, J.T., Riebe, C.S., Martel, S.J., Carr, B., Harman, C., Singha, K., deB Richter, D., 2015. Geophysical imaging reveals topographic stress control of bedrock weathering. Science (1979) 350, 534–538.

Stauffer, P.H., Auer, L.H., Rosenberg, N.D., 1997. Compressible gas in porous media: a finite amplitude analysis of natural convection. Int J Heat Mass Transf 40, 1585–1589. https://doi.org/https://doi.org/10.1016/S0017-9310(96)00222-0

Taillefer, A., Guillou-Frottier, L., Soliva, R., Magri, F., Lopez, S., Courrioux, G., Millot, R., Ladouche, B., Le Goff, E., 2018. Topographic and Faults Control of Hydrothermal Circulation Along Dormant Faults in an Orogen. Geochemistry, Geophysics, Geosystems 19, 4972–4995. https://doi.org/10.1029/2018GC007965

Tarcan, G., Gemici, Ü., Aksoy, N., 2005. Hydrogeological and geochemical assessments of the Gediz Graben geothermal areas, western Anatolia, Turkey. Environmental Geology 47, 523–534. https://doi.org/10.1007/s00254-004-1174-1

Tester, J.W., 2007. The future of geothermal energy, impact of Enhanced Geothermal Systems (EGS) on the United States in the 21st century: An assessment by an MIT-led interdisciplinary panel. Idaho National Laboratory, Idaho Falls.

Tezcan, A.K., Turgay, M.I., 1991. Heat flow and temperature distribution in Turkey, in: Cermák, V., Haenal, R., Zui, V. (Eds.), Geothermal Atlas of Europe. Herman HAACK Verlag, Gotha, Germany.

Tóth, J., 1999. Groundwater as a geologic agent: An overview of the causes, processes, and manifestations, Hydrogeology Journal. Springer-Verlag.

Ünsal, N., Afşin, M., 1999. Hydrochemical and isotopic properties of the Mahmutlu and Bağdatoğlu mineralized thermal springs, Kırşehir, Turkey. Hydrogeol J 7, 540–545.

Uzelli, T., Bilgiç, E., Öztürk, B., Baba, A., Sözbilir, H., Tatar, O., 2021. Effects of seismic activity on groundwater level and geothermal systems in İzmir, western Anatolia, Turkey: The case study from October 30, 2020 Samos earthquake. Turkish Journal of Earth Sciences 30, 758–778. https://doi.org/10.3906/YER-2101-9

Vaught, T.L., 1980. An assessment of the geothermal resources of Illinois based on existing geologic data. Arlington, Virginia.

Vieira, F.P., Hamza, V.M., 2011. Global heat flow: Comparative analysis based on experimental data and theoretical values, in: 12th. International Congress of the Brazilian Geophysical Society. Society of Exploration Geophysicists, Rio de Janeiro, Brazil, pp. 1975–1979. https://doi.org/10.1190/sbgf2011-407

Wisian, K.W., Blackwell, D.D., 2004. Numerical modeling of Basin and Range geothermal systems. Geothermics 33, 713–741. https://doi.org/10.1016/j.geothermics.2004.01.002

Yildirim, C., Schildgen, T.F., Echtler, H., Melnick, D., Strecker, M.R., 2011. Late Neogene and active orogenic uplift in the Central Pontides associated with the

North Anatolian Fault: Implications for the northern margin of the Central Anatolian Plateau, Turkey. Tectonics 30. https://doi.org/10.1029/2010TC002756

Yurteri, C., Simsek, S., 2017. Hydrogeological and hydrochemical studies of the Kaman-Savcili-Büyükoba (Kirsehir) geothermal area, Turkey. Geothermics 65, 99–112. https://doi.org/10.1016/j.geothermics.2016.09.002

Zengin, E., 2014. Aksaray ilindeki jeotermal enerji kaynaklarının potansiyeli ve ısıtma sisteminde kullamına yönelik araştırmalar (Master's Theis). Aksaray Üniversitesi, Fen Bilimleri Enstitüsü, Aksaray.

APPENDICES

APPENDIX A. Numerical modeling outcomes in FlexPDE

A.1. Model geometry of H=500 m, model domains and e-profile location

The geometry of the model considered in FlexPDE domain is a cross-section of typical fault-controlled geothermal systems in CA Region, length as 23 km and breadth as 20 km. However, since, an H is in the upper boundary, the breadth is higher than 20 km. The breadth varies based on the H scenario, whereas the length is constant throughout the study. In addition, the designated length is sufficient for convection in a geothermal system for the fluid circulation. All boundaries of the model are clearly illustrated in different colours as shown in **Figure A.1**. In addition, location of e-profile as a vertical profile, representing a synthetic vertical borehole is demonstrated in **Figure A.1**.

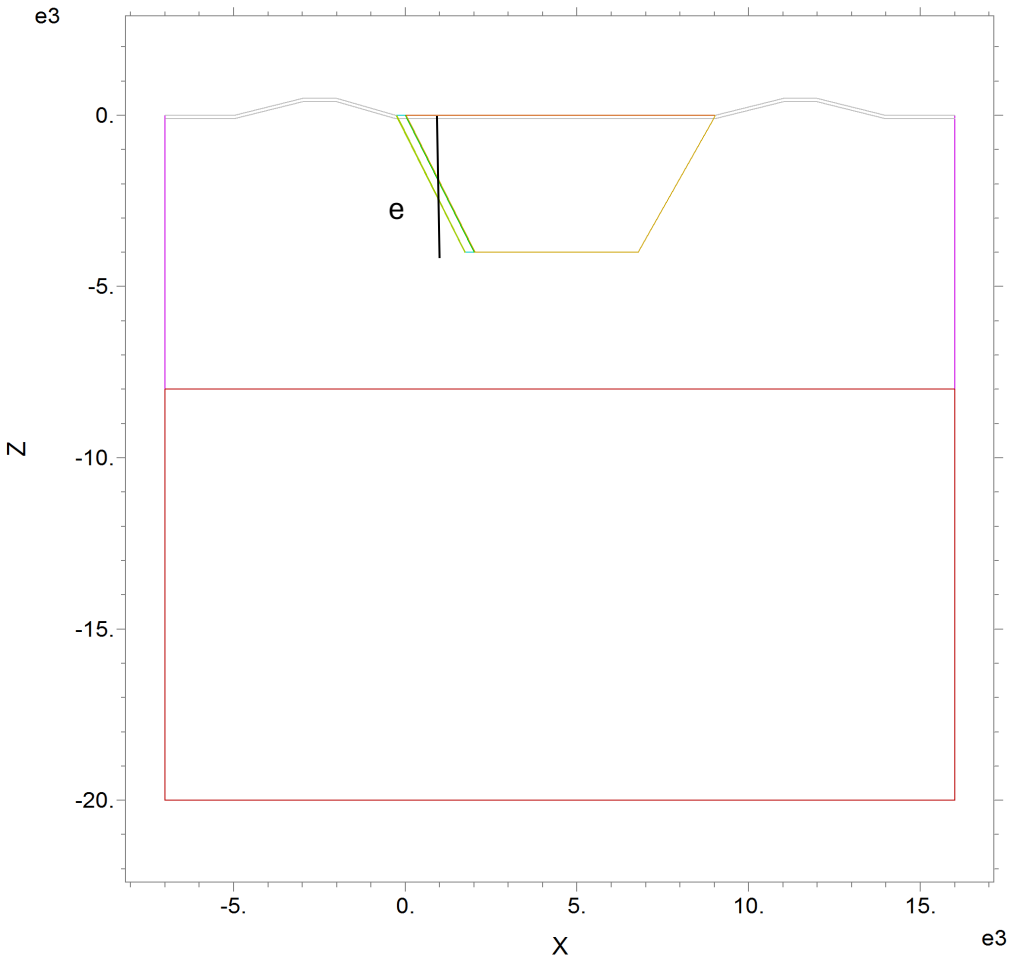

Figure A.1 Model geometry of H=500 m and e-profile.

A.2. Meshing of H=500 m and K_2=10^{-16} m^2 scenario

In FlexPDE, the program itself runs auto mesh for boundary conditions and domains designated in the script code. It is observed that the nodes and cells used in calculation of numerical model in FlexPDE are based on the inputs such as geometry, boundary conditions, equations, parameters, and outcome reports produced after script code is fed and FlexPDE runs to calculate using FEM, producing mesh for each boundary. Different colours show various zones of the model. High mesh density was observed in and around the fault zone region and upper boundary. The mesh produced for H=500 m and K_2=10^{-16} m^2 is in **Figure A.2**. For H=0 m, at least 2423 nodes and 4651 cells were involved, the number of nodes and cells increase as the geometry is enlarged and parameter values are increased.

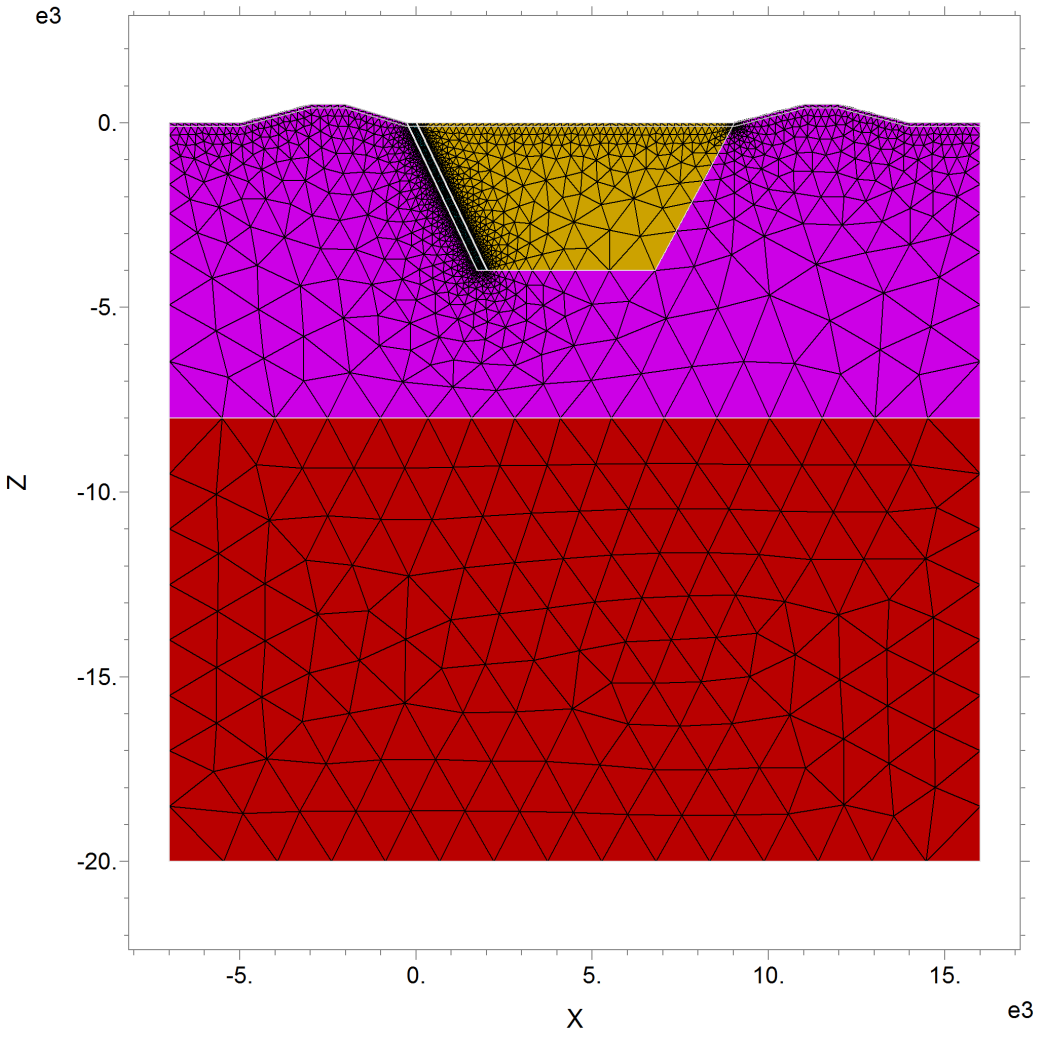

Figure A.2 An auto mesh in FlexPDE for H=500 m and K_2=10^{-16} m^2.

A.3. Temperature distribution scenario

Temperature distribution was previously discussed in this study, however FlexPDE output results were not demonstrated extensively. In this study, two clusters of basal heat flow were studied, KM (Q_b=110 mW·m^{-2}) and CAP (Q_b=65 mW·m^{-2}). The KM temperature distribution of H=500 m and K_2=10^{-16} m^2 is shown in Figure A.3. In **Figure A.3**, the upper boundary, T_0=20 °C, is contained and a slight upwards temperature isotherms are observed along the upper parts of the fault zone. Whereas the temperature at the bottom of the model is 905 °C. In addition, temperature distribution is evident in the basin of the model and flat temperature isotherms are observed at the bottom of the basement where a constant basal heat flux of Q_b=110 mW·m^{-2} has been applied uniformly at the base of the model, as the uniform temperature distribution is evident in **Figure A.3**.

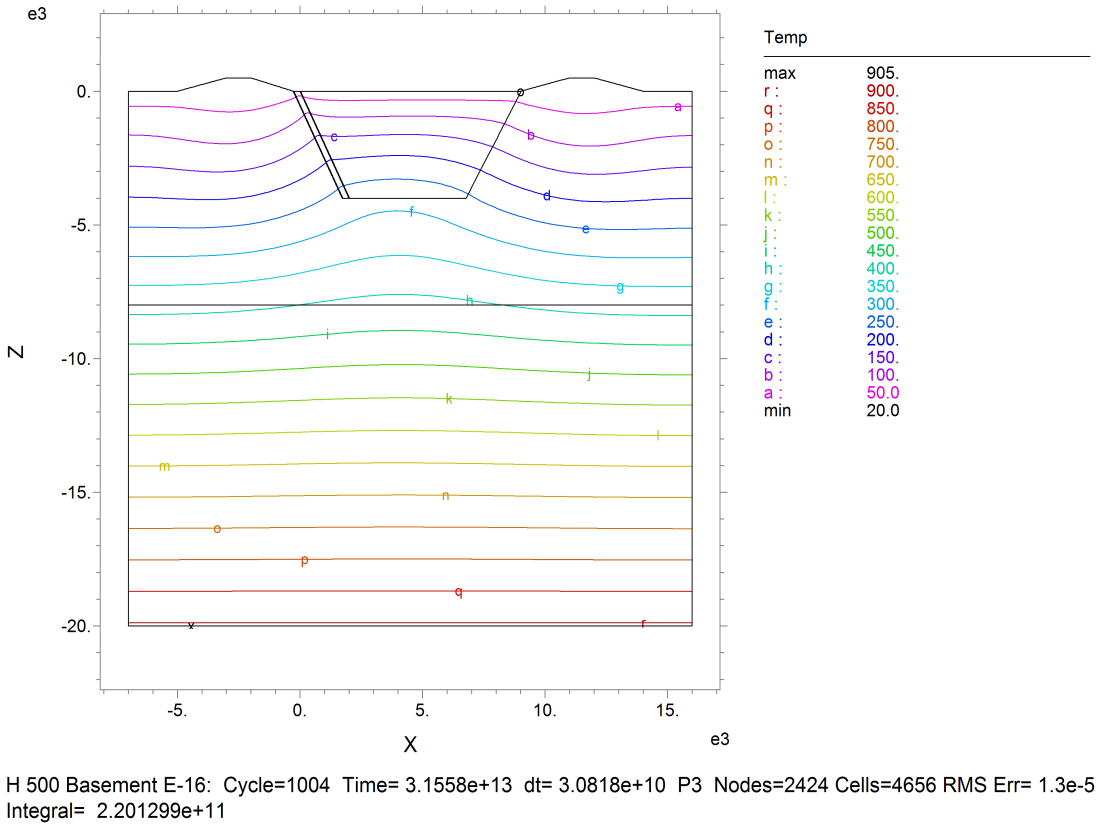

Figure A.3 Temperature distribution of KM at H=500 m.

A.4. Fluid velocity and circulation scenario

The fluid velocity is calculated in FlexPDE, and the outcome produced result provides an insight of fluid behaviour in geothermal systems. In **Figure A.4**, it is observed that fluid circulation is recharged from highest elevation of topography, finding pathway to the fault zone and eventually discharges from the model as, K_2=10^{-16} m^2. The fluid velocity is maximum in fault zone, 2.25x10^{-9} $m{\cdot}s^{-1}$, particularly in the top fault and minimum fluid velocity is in the deeper subsurface layers. Red arrows represent high fluid velocity, blue arrows represent medium fluid velocity and purple arrows represent no fluid velocity in **Figure A.4**.

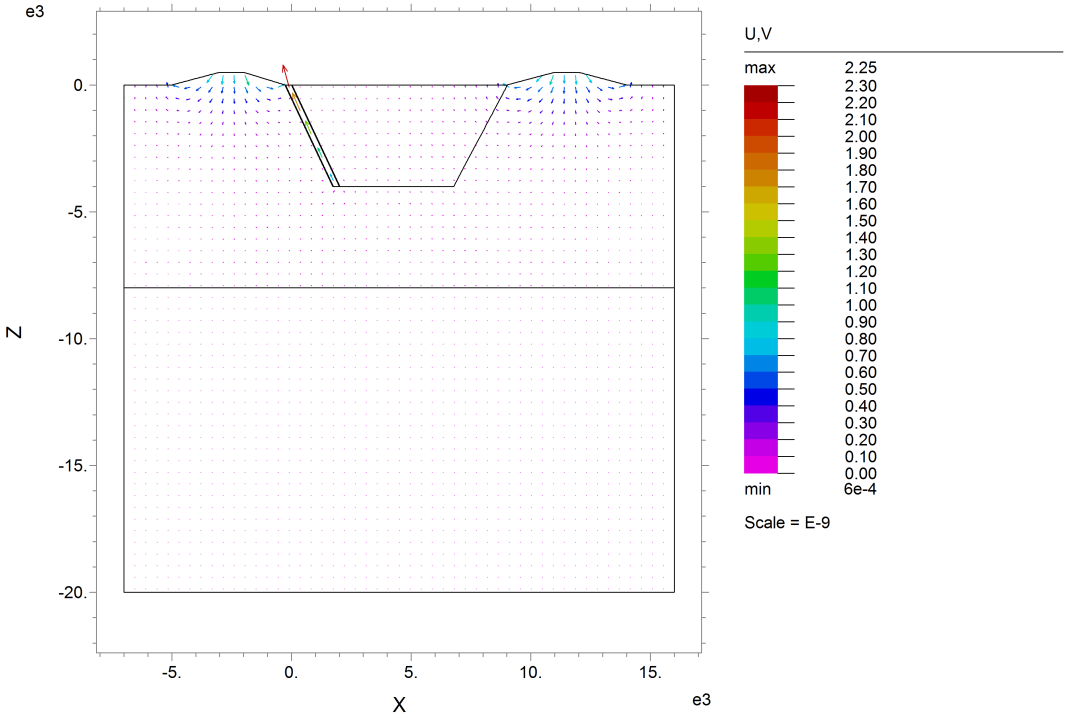

Figure A.4 Fluid velocity and fluid circulation produced for H=500 m in KM.

A.5. Fluid velocity in low topographic relief

In low or no topographic relief, such as H=0 m, fluid velocity is lower and fluid circulation is minimal. In addition, the fluid recharge location is undefined in the domain in **Figure A.5**. The fluid discharge is observed in the fault zone in **APPENDIX A.4**.

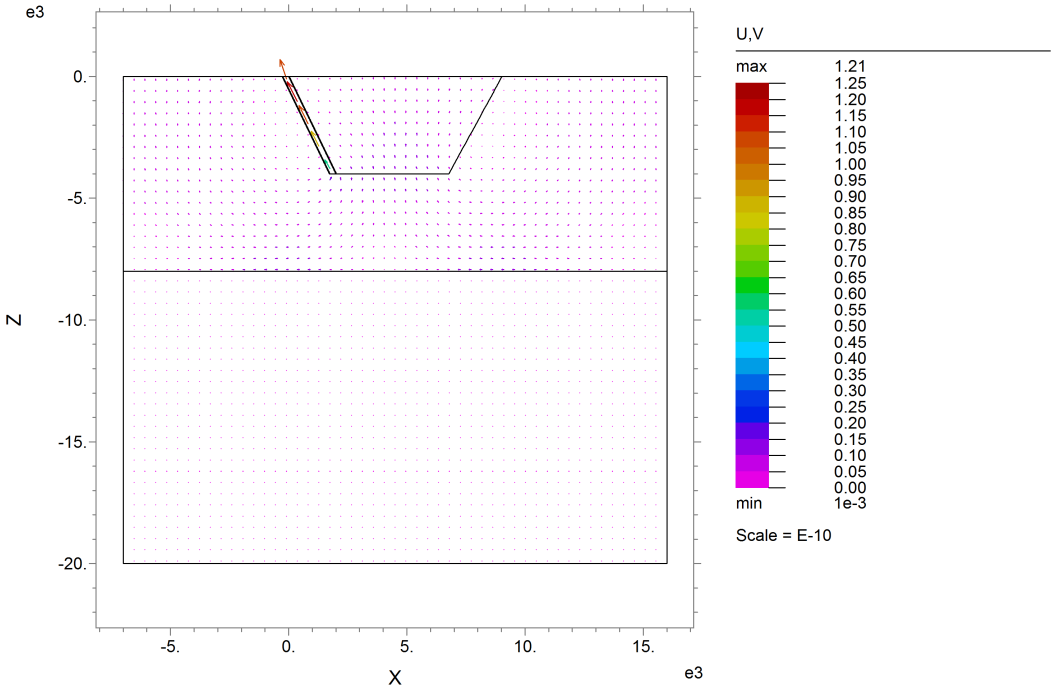

Figure A.5 Fluid velocity and fluid circulation produced for H=0 m, K_2=10^{-16} m^2 in KM.

A.6. Pressure distribution

The pressure distribution shows that in deeper subsurface layers, the pressure is higher compared to upper subsurface layers. In addition, the maximum bottom boundary pressure is calculated as 2.01×10^8 Pa. The red represents higher pressure values and purple represents lower pressure values in **Figure A.6**.

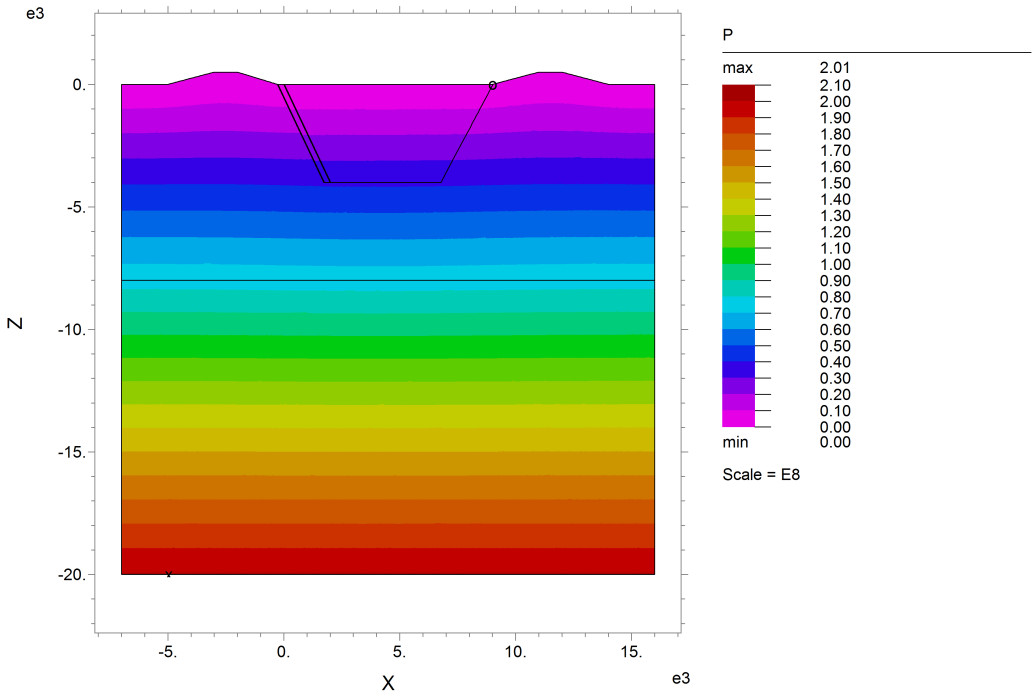

Figure A.6 Pressure distribution for H=500 m, K_2=10^{-16} m^2 in KM.

APPENDIX B. Validation of produced models

B.1. Temperature distribution validation results

Two different bedrock permeability values a) K_2=10^{-18} m^2 (top panels) and b) K_2=10^{-16} m^2 (bottom panels) were produced for the validation of the finite element model. The panels on left show results produced by (Wisian and Blackwell, 2004) using TOUGH2. The panels on right show results produced within the scope of this study using FlexPDE. In FlexPDE models, a 12 km thick impermeable layer, K=10^{-20} m^2, was used at the bottom to provide base heat flow as shown in **Figure B.1**. The basal heat flow in **Figure B.1** of right panels is Q_b=65 $mW \cdot m^{-2}$, CAP of CA Region.

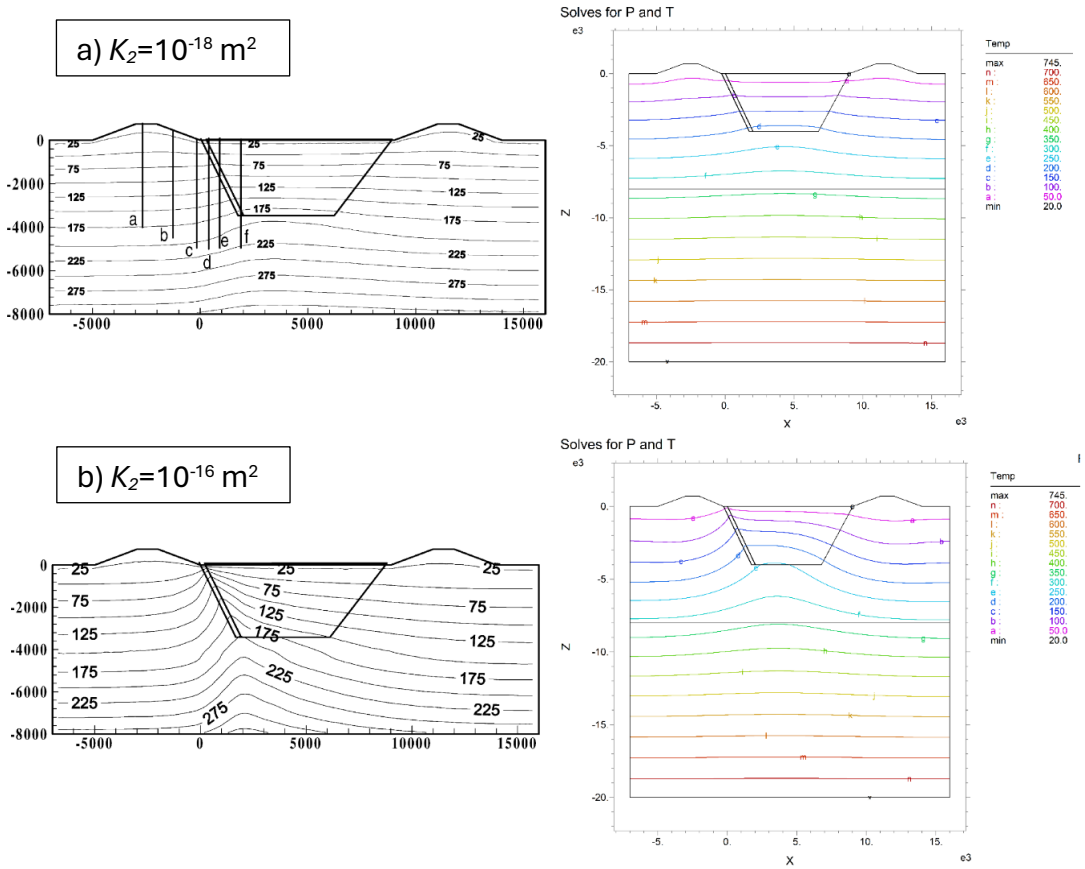

Figure B.1 Temperature distribution validation results for a) K_2=10^{-18} m^2 and b) K_2=10^{-16} m^2.

APPENDIX C. Elevation profiles of CA Region geothermal fields

C.1. Radius of Büyükoba-Savcılı

Prior to delineation of elevation profile, a radius of ~5 km is encircled from the geothermal source using Google Earth tools. The elevation profile is delineated from one point of circle to another point of circle for ~10 km in elevation profile. The area of geothermal system is encircled in red is Büyükoba-Savcılı geothermal field in **Figure C.1**.

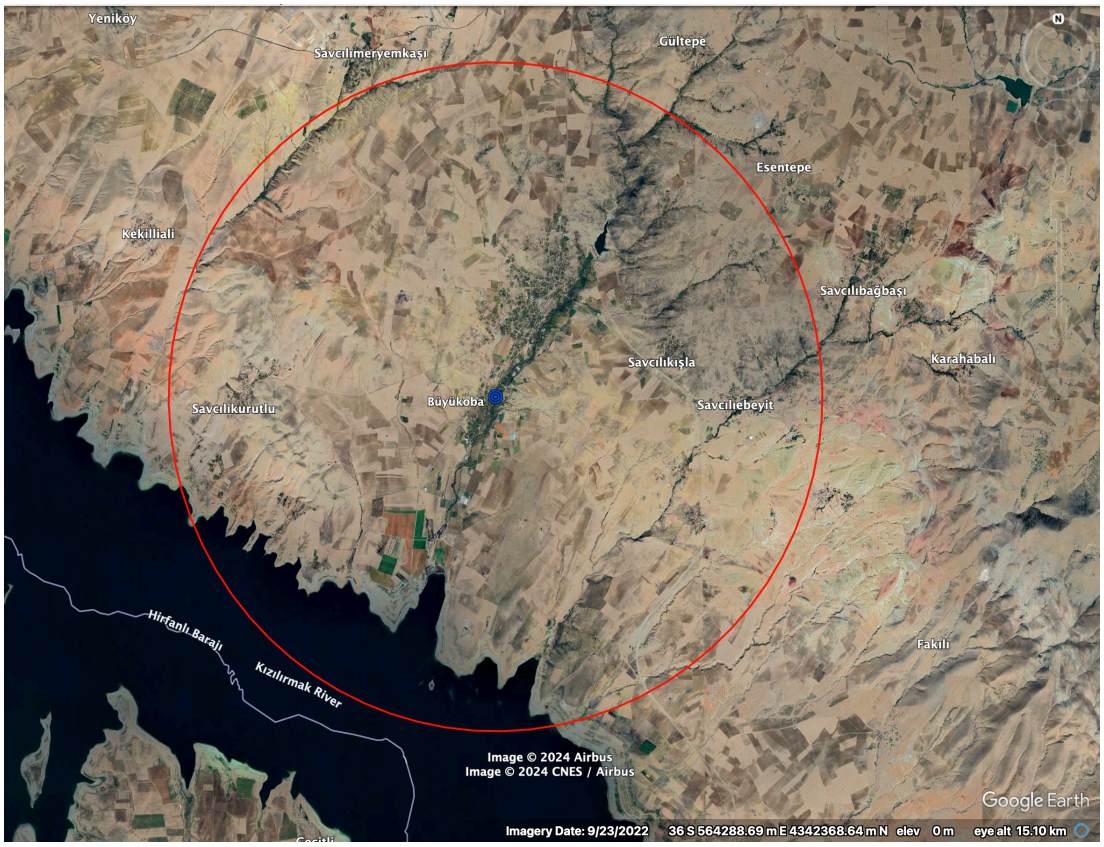

Figure C.1 Encircled area of Büyükoba-Savıcılı geothermal field.

C.2. Elevation profile of Büyükoba-Savcılı

Many elevation profiles were delineated in the area to retrieve the maximum H suggested in the geothermal field. The maximum H was then employed in the calculations of this study. The elevation profile is delineated using the Google Earth, line option, to produce the profile. The elevation profiles are approximately 10 km in distance, and proportional to fault lines in the vicinity of the geothermal source. The geothermal source location is indicated, dark blue circle, red arrow is the point where the location of geothermal source corresponds in the elevation profile as shown in **Figure C.2**.The maximum height in the profile is 1107 m, and minimum height is 877 m, above sea level, where H=230 m.

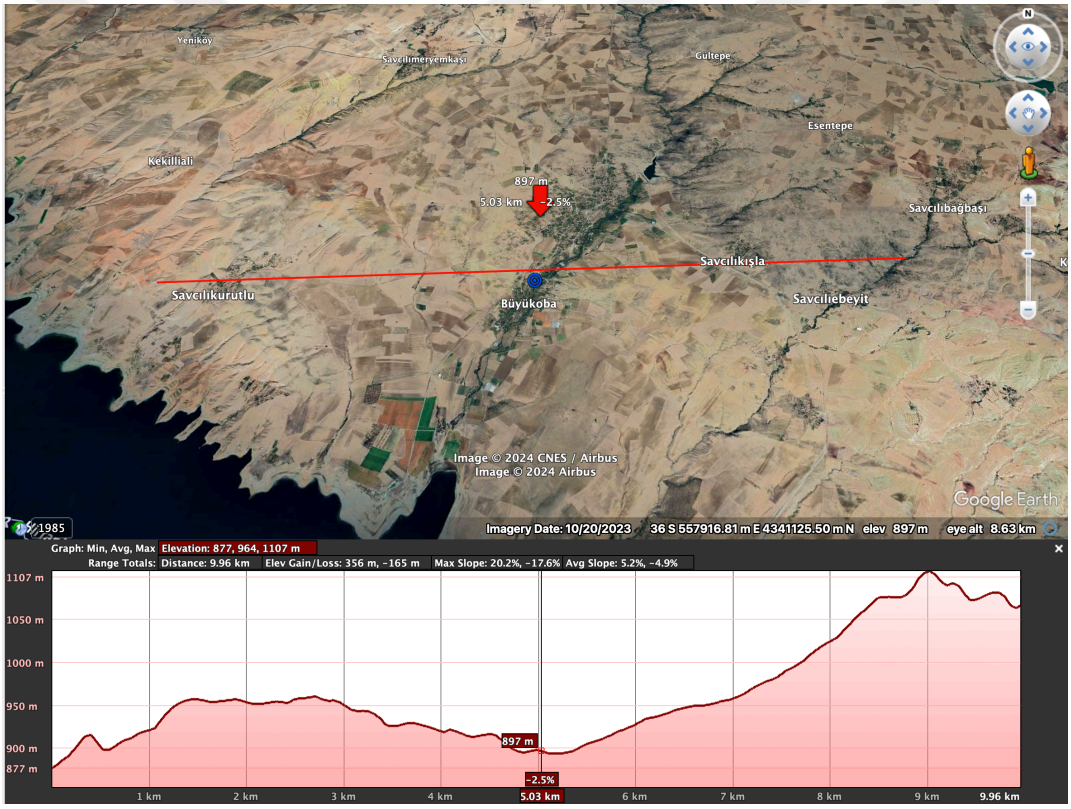

Figure C.2 An elevation profile of Büyükoba-Savcılı geothermal field.

C.3. Radius of Çiftehan

Similar to the procedure in **APPENDIX C.1**, the area of Çiftehan is encircled in red in **Figure C.3**.

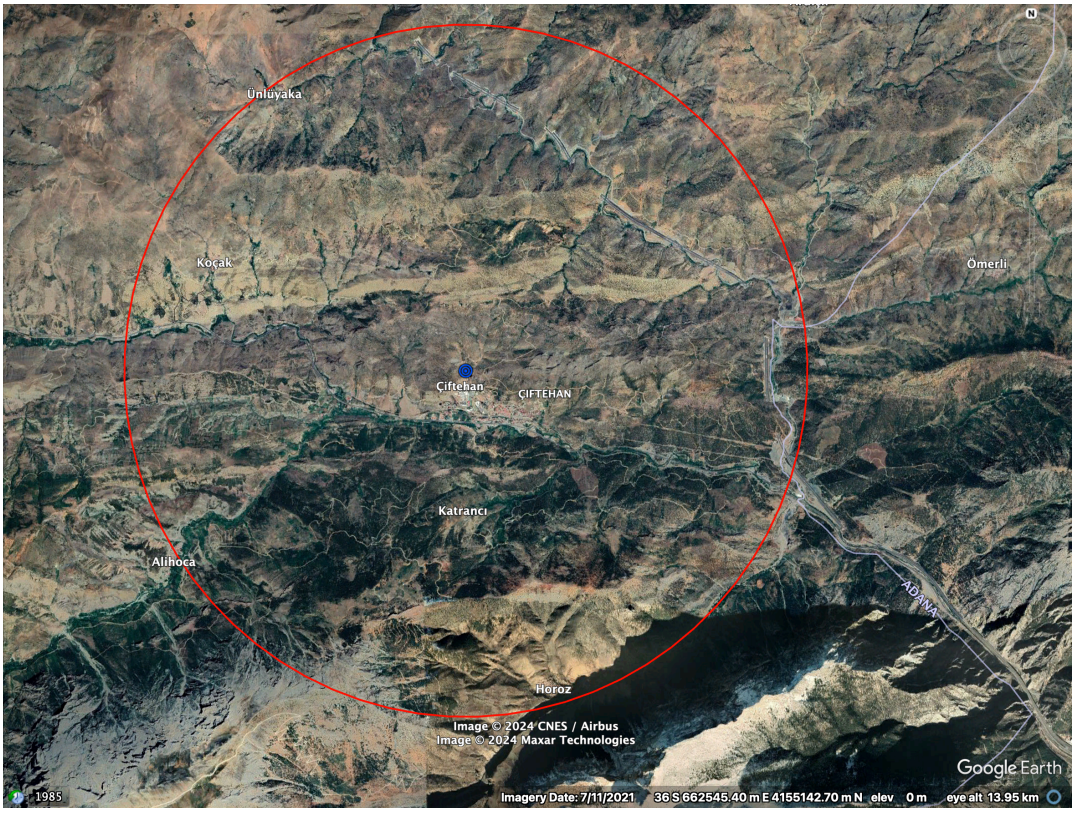

Figure C.3 Encircled area of Çiftehan geothermal field.

C.4. Elevation profile of Büyükoba-Savcılı

The same method employed in **Figure B.1** is implemented in Çiftethan geothermal field. The maximum height in the elevation profile is 2200 m, and minimum height is 951 m above sea level, where H=1049 m in **Figure C.4**.

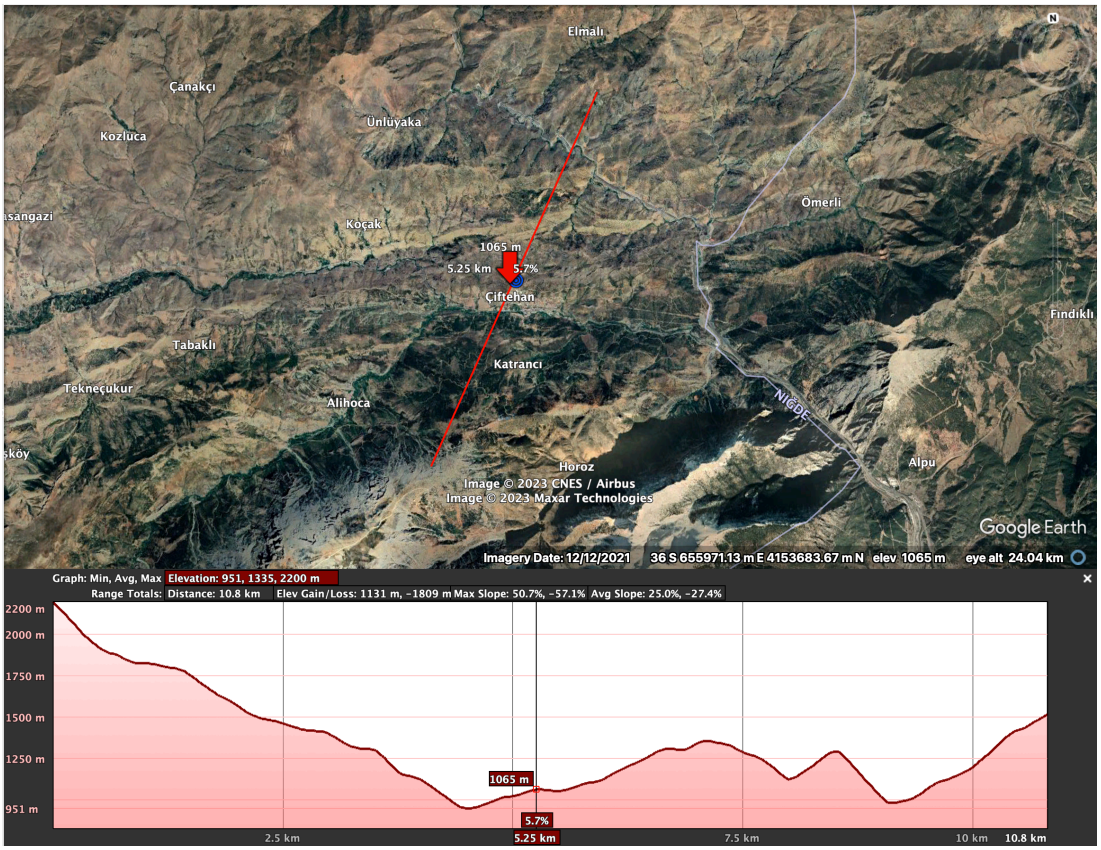

Figure C.4 An elevation profile of Çiftehan geothermal field.

CURRICULUM VITAE

Sinan BURHAN

Education: MSc in Environmental Engineering 2020-Present

Marmara University, Istanbul

MSc in Engineering Management (non-thesis) 2019-2020

Marmara University, Istanbul

BSc in Civil Engineering 2014-2018

Hasan Kalyoncu University, Gaziantep

Experience: Research Scholar January 2023-May 2023

TÜBİTAK, Marmara University

Project: Investigation of the relationship between the topographic and the fluid circulation depth on the geothermal systems of Central Anatolia Region

Engineering Intern January 2018-May 2018

Punj Lloyd-Limak-Kalyon Joint Venture, Ankara

Project: TANAP Natural Gas Pipeline

Programs: AutoCAD, MathCAD, NetCAD, SAP2000, ArcGIS, SimaPro, FlexPDE, Plaxis2D, Microsoft Office and Primavera

Languages: English, Turkish, Arabic, Persian, Urdu

Achievements: Department 3rd position, BSc in Civil Engineering

Erasmus Scholarship, Warsaw University of Technology, BSc in Civil Engineering

Conferences: 14th International Exergy, Energy and Environment Symposium (IEEES-2023) – Piri Reis University, Istanbul

Certificates: ISO 45001: 2018, ISO 14001: 2015 and ISO 9001: 2015